Development and Characterisation of Completely Degradable Composite Tissue Engineering Scaffolds

PhD Thesis by Montse Charles-Harris Ferrer

PhD Supervisor: Josep A. Planell i Estany

Barcelona, July 2007

Chapter 3. Development and optimisation of biodegradable composite scaffolds via Phase Separation

Introduction

As was discussed in the Introduction (Chapter 1), thermally induced phase separation was first applied to PLA scaffolds by Schugens et al. [1;2], and several authors have applied this technique to composite scaffolds [3-6]. Phase separation can be induced in several ways: thermally induced phase separation, non-solvent induced phase separation and chemically induced phase separation. Thermally induced phase-separation is induced by changes in the solubility and Gibbs free energy of a two-phase system with temperature. Non-solvent induced phase-separation is a ternary system involving the polymer, a solvent and a non-solvent. Phase-separation is induced by adding the non-solvent into the polymer and solvent solution. Chemically induced phase-separation occurs in systems consisting of a non-reactive polymer and a monomer that undergoes condensation polymerization. After phase separation and appropriate treatment to eliminate the second phase if necessary, a porous network is obtained [7;8].

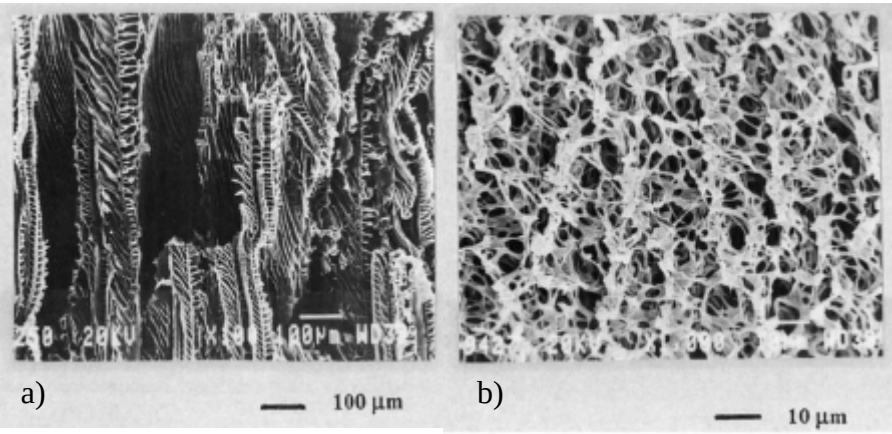

Figure 3.1: SEM images of PLA/dioxane scaffolds showing: a) typical solid-liquid phase separation morphology, and b) typical liquid-liquid spinodal decomposition morphology (b). From [1].

The technique used in this study is thermally induced phase separation and will thus be discussed in further detail. Thermally induced phase separation can be either liquid-liquid or solid-liquid. Liquid-liquid phase separation occurs when the temperature of the solution decreases below the binodal decomposition temperature (Figure 3.2). Below this temperature, the solubility of the phases decreases and the solution is driven towards a separation into a polymer-rich phase and a polymer-poor phase (i.e. the solvent). Gelation occurs at low quenching rates and in the presence of H_2O. The distribution of each phase will depend on the concentration of polymer in the solution. Thus at low polymer concentrations (Figure 3.2a), polymer droplets disperse within the matrix of the solvent leaving behind a polymer powder after solvent removal. At high polymer concentrations (Figure 3.2c) the solvent forms droplets within the polymer matrix creating a relatively closed-pore structure after solvent removal. Nucleation and growth is the expected mechanism when a system leaves the thermodynamically stable condition and slowly enters the metastable region of the phase diagram, between the binodal and the spinodal curves. Dispersed nuclei are formed and become stable if the activation energy for nuclei formation is higher than their surface free energy. Nucleation and growth is usually a slow process and leads to a disperse domains morphology[9;10].

At medium polymer concentrations (Figure 3.2b) below the spinodal curve, the solution forms an isotropic bi-continuous structure, usually by spinodal decomposition, of interconnected pores. Spinodal decomposition takes place in a fast quench into the two-phase region limited by the spinodal curve or even in a slower quench crossing the metastable region near the critical point. In this case, phase separation is initiated with concentration fluctuations of increasing amplitude, giving rise to two continuous phases, with a characteristic periodic interphase distance. If the process is ‘frozen’ early enough by a mobility change, a morphology with high interconnectivity is obtained. However, in the later stages of phase separation, coalescence may also take place, leading to a matrix/disperse domains morphology. Spinodal decomposition is normally much faster than nucleation and growth.

In the case of semi-crystalline polymers the polymer crystallisation may compete with the liquid-liquid phase separation. If both processes take place at similar

temperatures, the kinetics of each process will determine the outcome. In general, however, liquid-liquid phase separation is faster than polymer crystallisation.

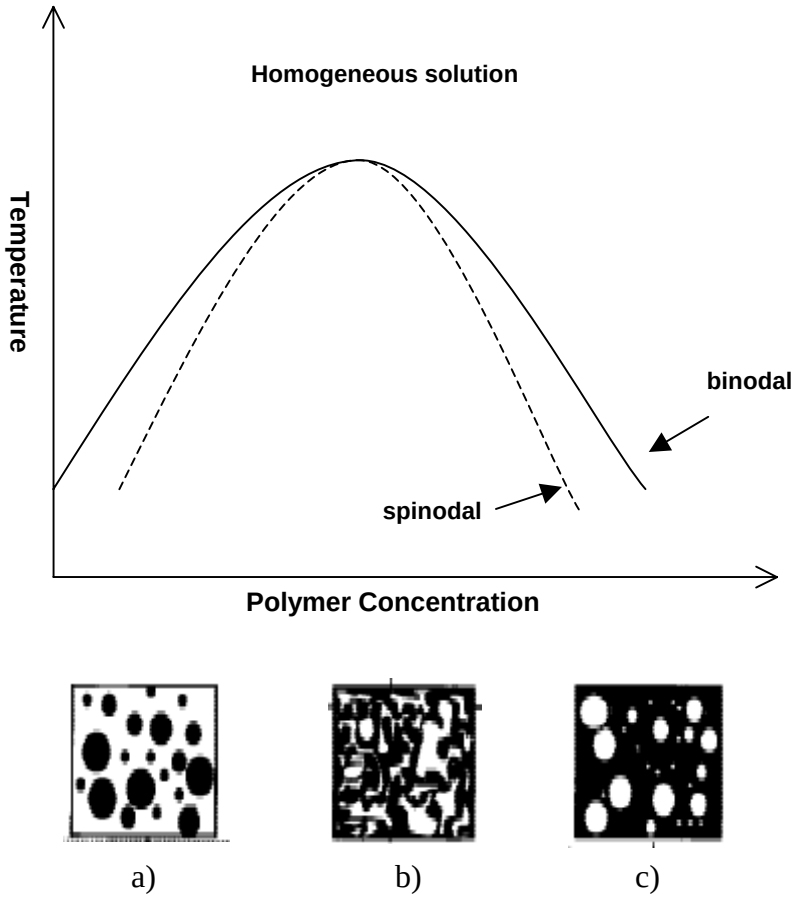

Figure 3.2: Schematic temperature-composition phase diagram of a polymer solution. Adapted from [8;11].

Solid-liquid phase separation takes place if the solvent crystallisation temperature is higher than the liquid-liquid phase separation temperature. As the temperature decreases, the solvent crystallises and expels the polymer from the crystallisation front. This process takes place by a nucleation and growth mechanism. The predominance of either nucleation or growth depends on the quenching temperature and on the quenching rate and nature of the polymer and solvent. Solid-liquid phase separation typically forms an anisotropic ladder-like structure, of more or less evenly spaced solvent crystals (Figure 3.1a). Therefore, the final phase-separated structure depends on the competing phase transition between the liquid/liquid phase separation

and the nature of the solidification process: vitrification, crystallisation of the polymer or freezing of the solvent.

After the solid-liquid or liquid-liquid decomposition, the solvent must be removed from the scaffold in order to obtain the porous structure. This removal must take place at a temperature below the solvent solidification curve in order to avoid the solvent re-dissolving the polymer. The removal is typically performed by freeze-drying, also called lyophilisation. During this process, the phase-separated mixture is maintained at low temperatures and a high vacuum is applied in order to sublime the solvent. Alternatively, the solvent can be extracted by soaking the mixture in a substance which dissolves the solvent but not the polymer. This method, called freeze-extraction, was applied to polymeric scaffolds by Ho et al. [12] using ethanol.

The phase separation processing parameters and the composition of the solution have a very strong influence on the morphology of the porous structures they create. Quenching at low temperatures reduces pore size due to the nucleation phenomena. Quenching at high temperatures, on the other hand, tend to create larger pores due to existence of less nulcei and the prevalence of the growth phenomena and the coalescence of the separated phase. The quenching rate and the temperature at which solvent removal takes place also affects pore size. Polymer concentration influences the density and thus the overall porosity of the structure. Both quenching parameters and polymer concentration influence the occurrence of liquid-liquid or solid-liquid phase separation. Semi-crystalline polymers tend to create more porous structures than their amorphous counterparts due to the higher contraction of the semicrystalline phase during solidification. Polymer molecular weight has not been found to have significant effects on the overall pore morphology[1;2;6;8;11;13]. Water is often added into the PLA/dioxane solution either to induce liquid-liquid phase separation[1], or to modulate pore size[11] and pore morphology[13]. Water is completely miscible in dioxane but does not dissolve PLA, thus reducing the solubility of the PLA in the solvent.

1,4-dioxane is often used as the solvent when creating PLA phase-separated scaffolds. Its physical properties are very convenient for this procedure because it is a PLA solvent and has a high melting point and a low boiling point, 11.8°C and 102°C respectively [14]. These temperatures allow for thermally induced phase separation at high temperatures, and facilitate sublimation. The use of dioxane in tissue engineering

systems is criticised by some authors because it is toxic and is a potential carcinogen, dimethylcarbonate has been used as an alternative solvent[15-17].

In this study, a thermally induced phase separation procedure has been developed and applied to the P-LL/DL-LA/G5 glass composite materials in order to manufacture scaffolds with high porosities and mechanical properties. This involved the preliminary tests, the development of the moulds or moulding procedure and the study of the composition. The processing parameters have been optimised in order to modulate porosity and pore size. The effects of the composition and the processing parameters on the scaffolds properties have been assessed by means of an experiment design.

Materials

Scaffold manufacturing

The scaffold materials: PLA and G5 glass, have been described in detail in Chapter 2. The solvent used in this case was 1,4-dioxane (Panreac Química, Spain), with 99.5% purity, stabilised with 25ppm butylated hydroxyl-toluene (BHT) and distilled water. The water was distilled with a Millipore Elix3.

The PLA pellets are dissolved in a 1,4-dioxane/water solution at different weight/volume (w/v%), this is done with a magnetic stirrer at 50°C. The water is previously mixed with the 1,4-dioxane at different volume/volume percent (v/v%). The dissolution takes approximately two days. If glass particles are added, they are added simultaneously with the PLA pellets in order to ensure homogeneous mixing. The solution is then poured into appropriate moulds, and quenched at low temperatures in order to induce the phase separation. The moulds are maintained overnight at this temperature. The dioxane is extracted either by freeze-drying or by solvent extraction with ethanol. In the former case, the samples are kept at -20°C or 0°C under vacuum (0.5 mmHg) to induce dioxane sublimation. In the latter case, the samples are soaked in chilled ethanol. For the preliminary study, the scaffolds were soaked in ethanol for two

days. In the optimisation study, the scaffolds were soaked in ethanol for three days, and the ethanol was changed thrice during this time.

Preliminary study with PLA scaffolds

Materials and Methods

The preliminary study on the composition and processing of the phase-separated scaffolds was developed by means of a four-factor factorial experiment design using only PLA (without adding the glass particles). The influence of four aspects of scaffold composition on the morphology and porosity of the scaffolds was studied. The four factors were: a) w/v% of the PLA/dioxane solution, b) v/v% of water in the 1,4-dioxane/water solution, c) quenching temperature, and d) solvent removal method: freeze-extraction or freeze-drying. All factors, except the quenching temperature, were tested at two levels: a maximum (+1) and a minimum (-1). Three levels were used for the quenching temperature due to the large gap between the lower level temperature, -196°C and the upper level, 0°C (Table 3.1 and Table 3.2).

The moulds used for the preliminary study were made of aluminium foil and measured 1cm in diameter and 1cm in height. They could be easily peeled off after solvent extraction.

	w/v% of PLA	v/v% of H_2O in the solvent	Quenching temperature	Solvent removal method
Low level (-1)	2.5%	0%	A = (-196°C), B= -20°C	Freeze-extraction
High level (+1)	7.5%	5%	0°C	Freeze-drying

Table 3.1: Levels of the factors used for the preliminary experiment design.

Composition Nº	w/v% of PLA	v/v% of H_2O in the solvent	Quenching temperature	Solvent removal method
1F	-1	-1	-1_A	+1
2F	+1	-1	-1_A	+1
3F	-1	+1	-1_A	+1
4F	+1	+1	-1_A	+1
5F	-1	-1	+1	+1
6F	+1	-1	+1	+1
7F	-1	+1	+1	+1
8F	+1	+1	+1	+1
9F	-1	-1	-1_B	+1
10F	+1	-1	-1_B	+1
11F	-1	+1	-1_B	+1
12F	+1	+1	-1_B	+1
5E	-1	-1	+1	-1
6E	+1	-1	+1	-1
7E	-1	+1	+1	-1
8E	+1	+1	+1	-1
9E	-1	-1	-1_B	-1
10E	+1	-1	-1_B	-1
11E	-1	+1	-1_B	-1
12E	+1	+1	-1_B	-1

Table 3.2: Composition of the 20 samples used for the preliminary characterisation

Morphology

A qualitative study of the scaffold morphology was performed by Scanning Electron Microscopy (SEM) on a Jeol JSM-6400. Scaffold material was left in liquid nitrogen overnight in order to obtain a clean fragile surface when cutting. The materials were gold-sputtered under vacuum before viewing.

Porosity

The porosity of the scaffolds was measured by mercury pycnometry. The apparent density of the scaffold ($\rho_{scaffold}$) was measured by means of the volume of mercury it displaced when submerged. The porosity of the scaffold is calculated by dividing its apparent density by the density of the solid composite (ρ_{solid}):

$$\%Porosity = 100\left(1 - \frac{\rho_{scaffold}}{\rho_{solid}}\right) \qquad \{1\}$$

Measurements are presented as an average of three samples.

Results and Discussion

Morphology

Figure 3.3 and Figure 3.4 show SEM images of the morphology of the scaffolds made during the preliminary study. The scaffolds do not contain glass particles. Scaffolds quenched in liquid nitrogen (compositions 1-4F, Figure 3.3) have small pore sizes; approximately 5 μm, and were very brittle. They did not solidify as an entire sample, but instead broke into several pieces within the mould. They were thus difficult to prepare for SEM and porosity measurements. Compositions 1-4E were not produced due to these difficulties in handling.

Compositions 5-12E and 5-12F are shown in Figure 3.4. Several important features can be observed qualitatively from these images. First of all, comparisons between compositions made by solvent freeze-drying (F) or by solvent freeze-extraction (E) do not exhibit noticeable differences. Both methods seem to create identical scaffold morphologies, similar pore shapes and the effect of the variation of the composition is identical for both. Secondly, the presence of H_2O in the solvent creates a secondary microporosity within the pore walls (Figure 3.5).

Views of the scaffolds at low magnifications reveal the anisotropy of the pores and the presence of defects within the structure (Figure 3.6). These defects are due to the solidification of the mix and entrapped air bubbles. The aluminium foils moulds are very conductive, thus the solidification of the mix begins at the mould walls creating cavities towards the interior. The w/v% of PLA influences the prevalence of these defects within the scaffolds (Figure 3.7). Lower PLA w/v% produce scaffolds with more and larger defects than those with high PLA w/v%.

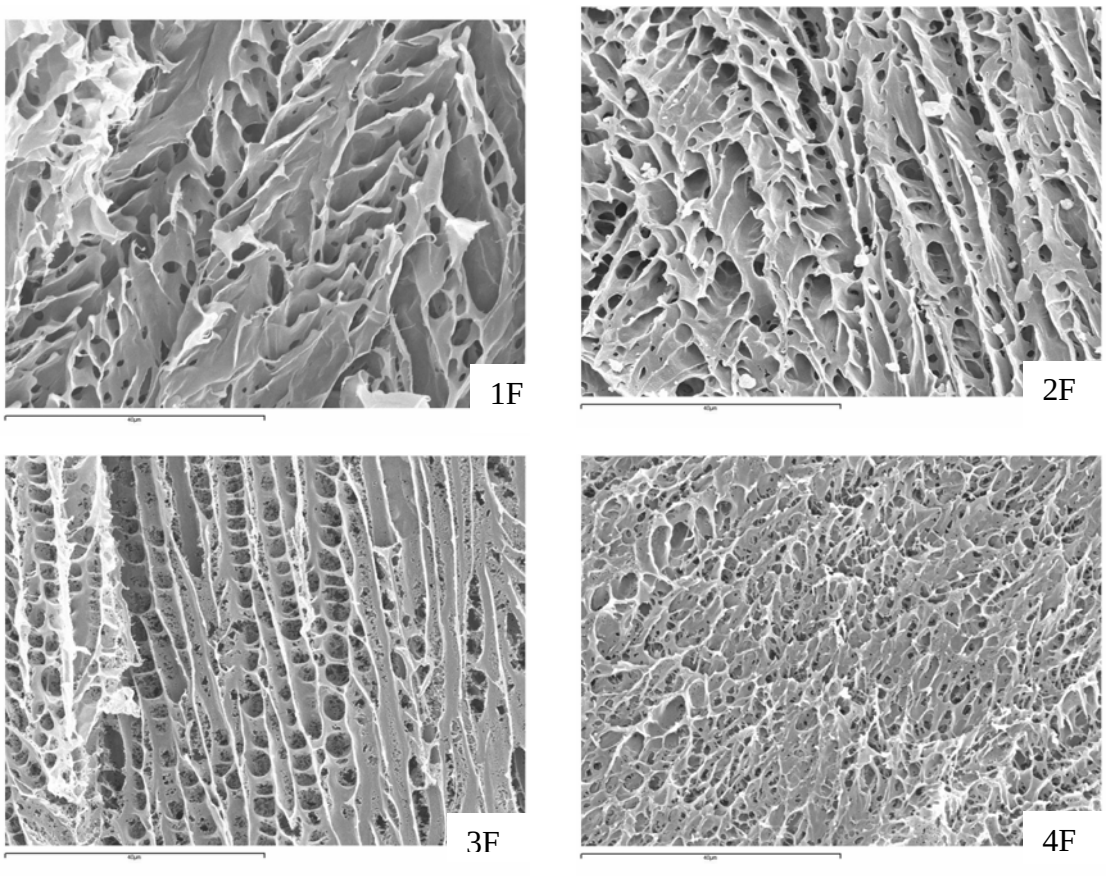

Figure 3.3: SEM images of compositions nº 1-4F, quenched in liquid nitrogen. These compositions had very small pore sizes (approx. 5 mm) and had large defects due to the harsh quenching conditions. (All magnification bars correspond to 40 μm)

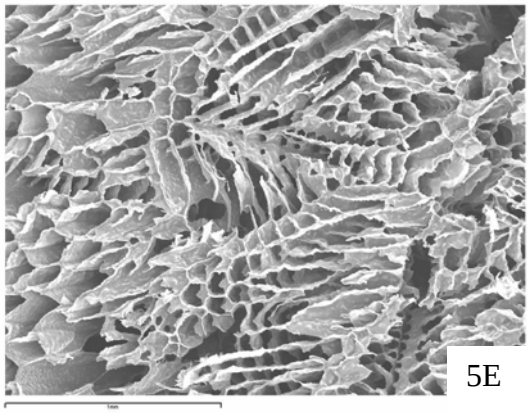
5E

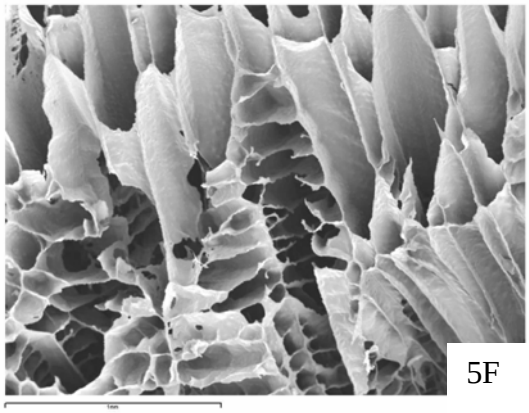
5F

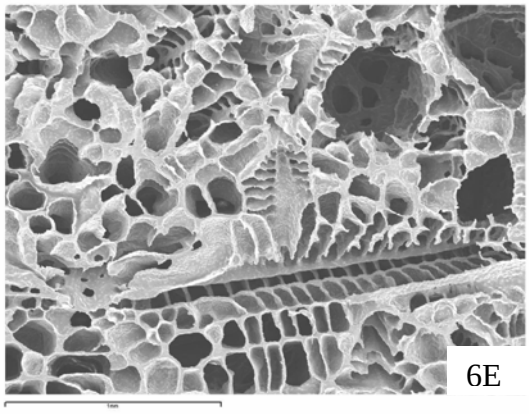
6E

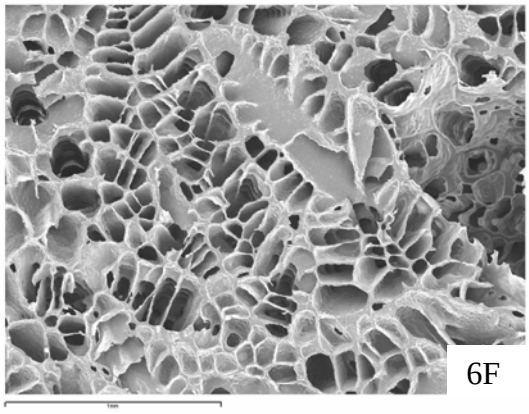
6F

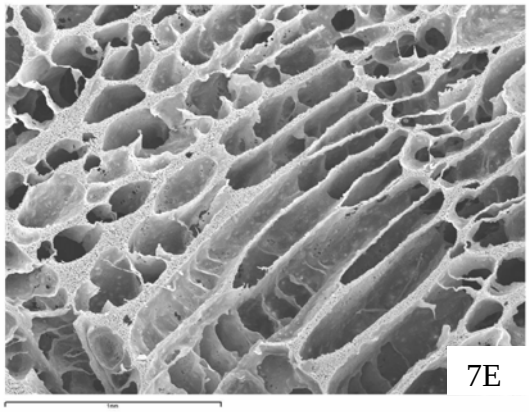
7E

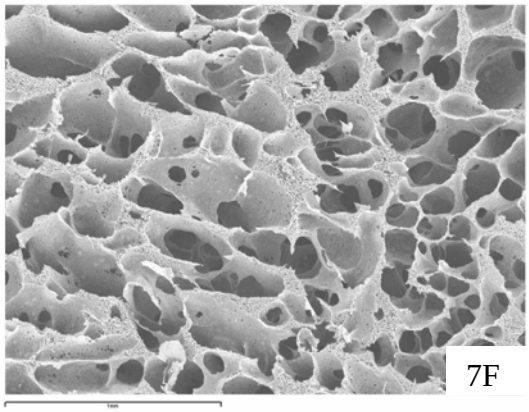
7F

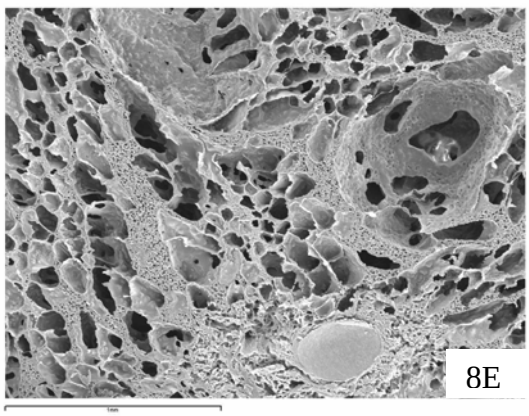
8E

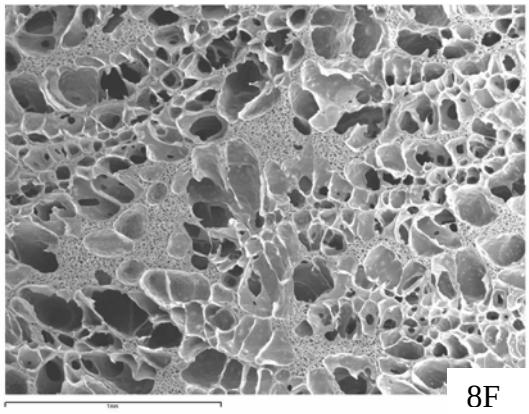
8F

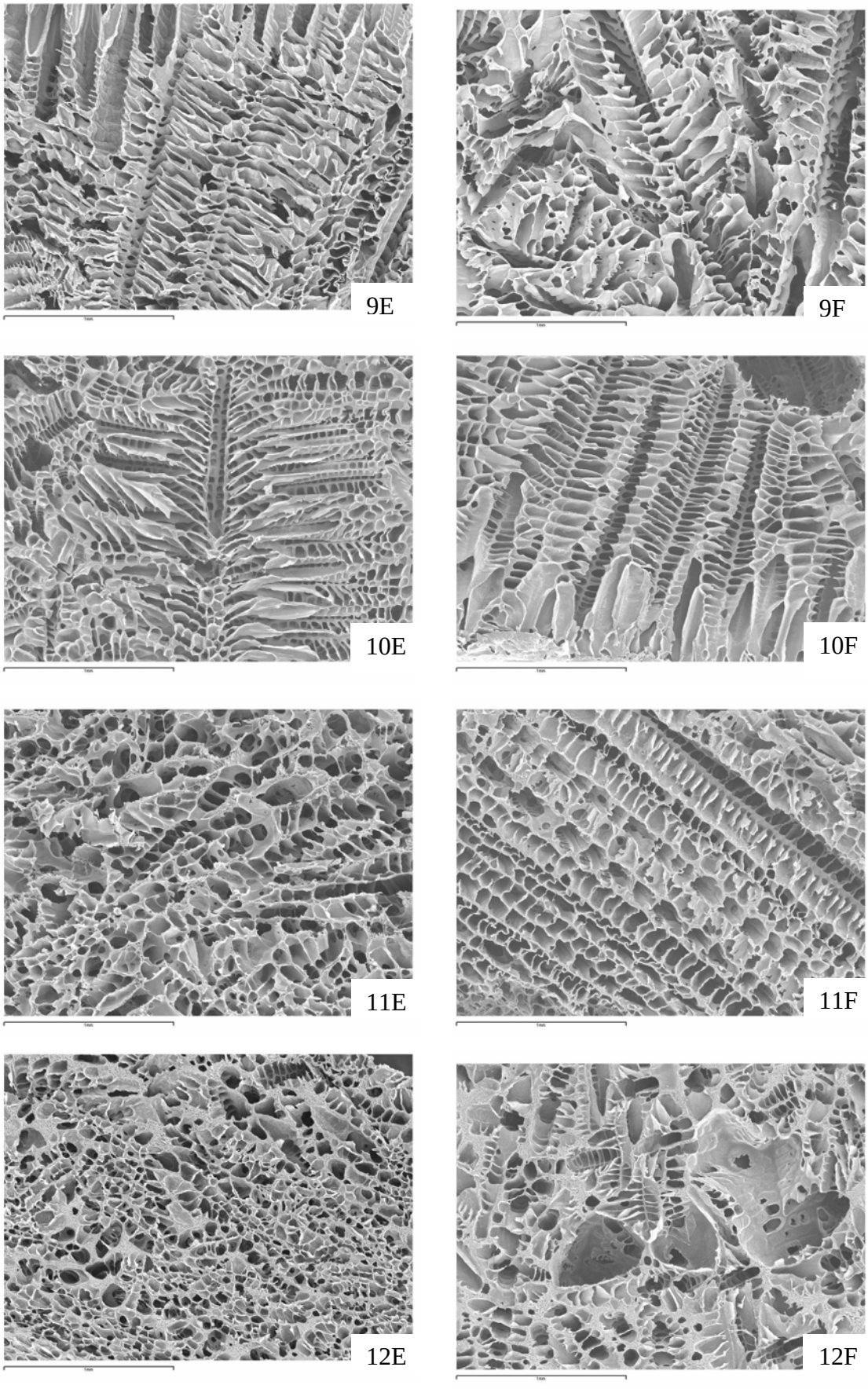

Figure 3.4: SEM images of compositions nº5-12E and nº 5-12 F. (All magnification bars correspond to 1mm)

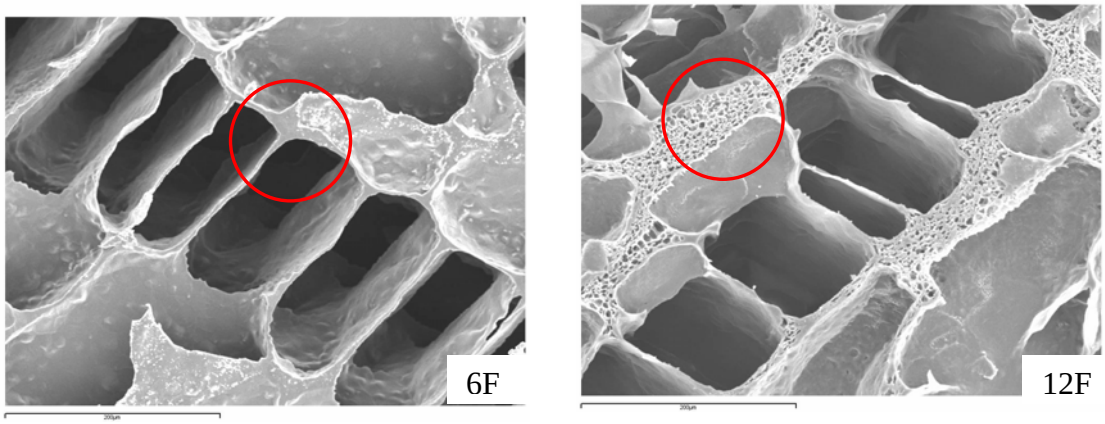

Figure 3.5: SEM images of compositions nº 6F and 12F. The microporosity within the pore wall created by the presence of H_2O is clearly visible in 12F. (Magnification bars correspond to 200μm)

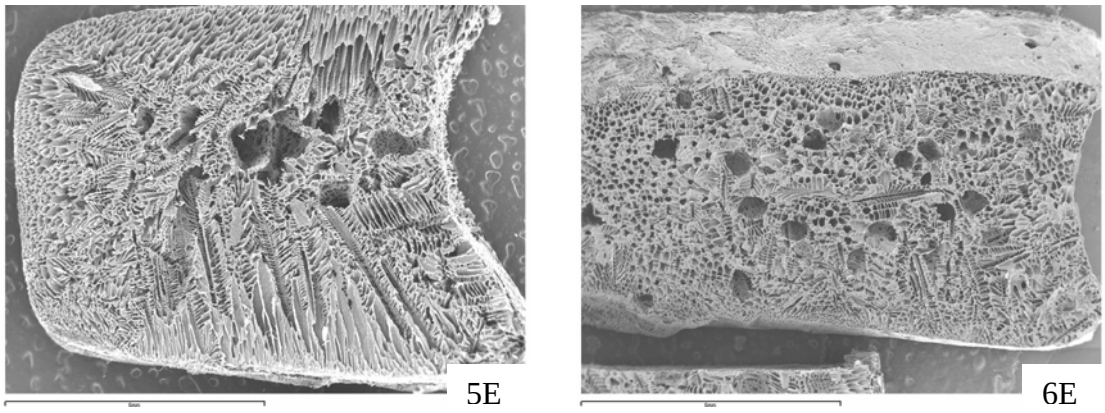

Figure 3.6: SEM images of compositions nº 5E and 6E. 5E shows the orientation of the pores from the walls of the mould towards the interior and the presence of the cavities. 6E shows less pore orientation and the presence of entrapped air bubbles within the structure. (Magnification bars correspond to 6mm)

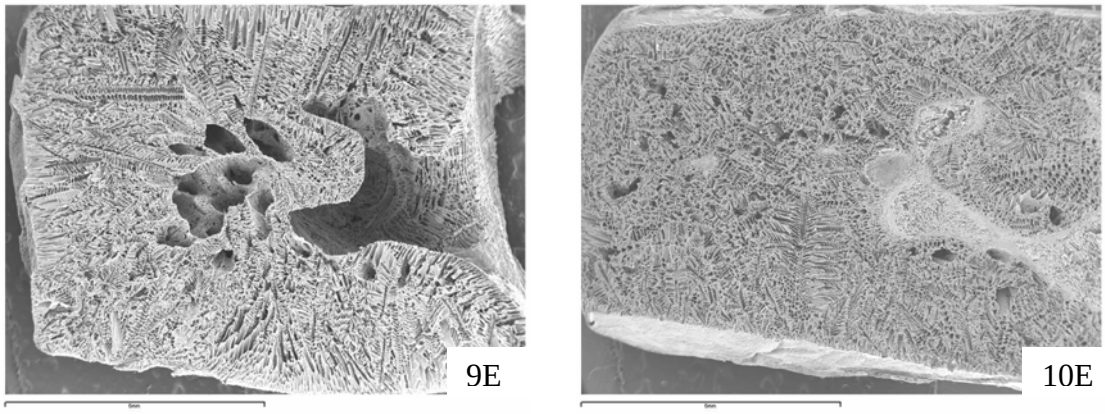

Figure 3.7: SEM images of compositions nº 9E and 10E illustrating the presence of large macroscopical defects in composition 9E which contains a smaller PLA w/v%. (Magnification bars correspond to 6mm)

Some compositions presented curious topographical features which can be seen at high magnifications (Figure 3.8). Indeed, the surface of the pore walls contain many hill-like structures will little peaks, which give the pore walls a micro/nano-roughness pattern. This phenomenon was reproducible: it occurred every time the scaffolds were produced, and is thus not due to an error or an random production condition. The close-up view reminds one of the typical nucleation and growth mechanism morphologies. It seems “grains” of polymer have nucleated and have grown into their neighbours[18].

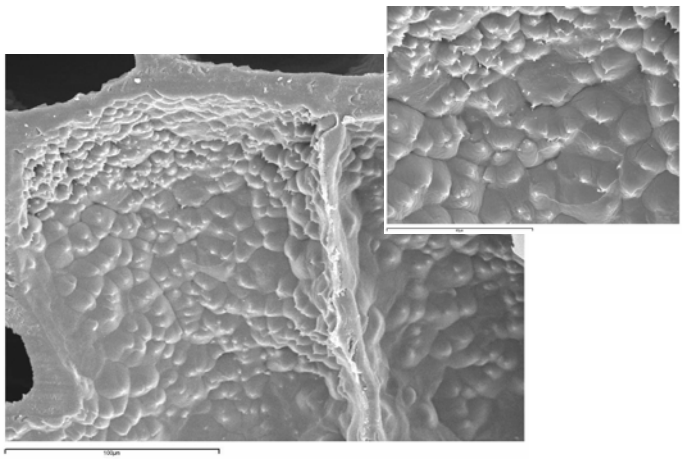

Figure 3.8: SEM images of composition nº 6E presenting micro-roughness on its pore walls. (The magnification bar of the main image (left) corresponds to 100 μm, in the close-up image (right) it corresponds to 40μm).

Porosity

The porosity results for composition 1-12 can be seen in Figure 3.9 (The numerical values can be seen in the Appendix Chapter 3). The porosity ranges between 82% and 96%. Compositions with low PLA w/v% (odd-numbered compositions) have higher porosities than those with the high level of PLA w/v%.

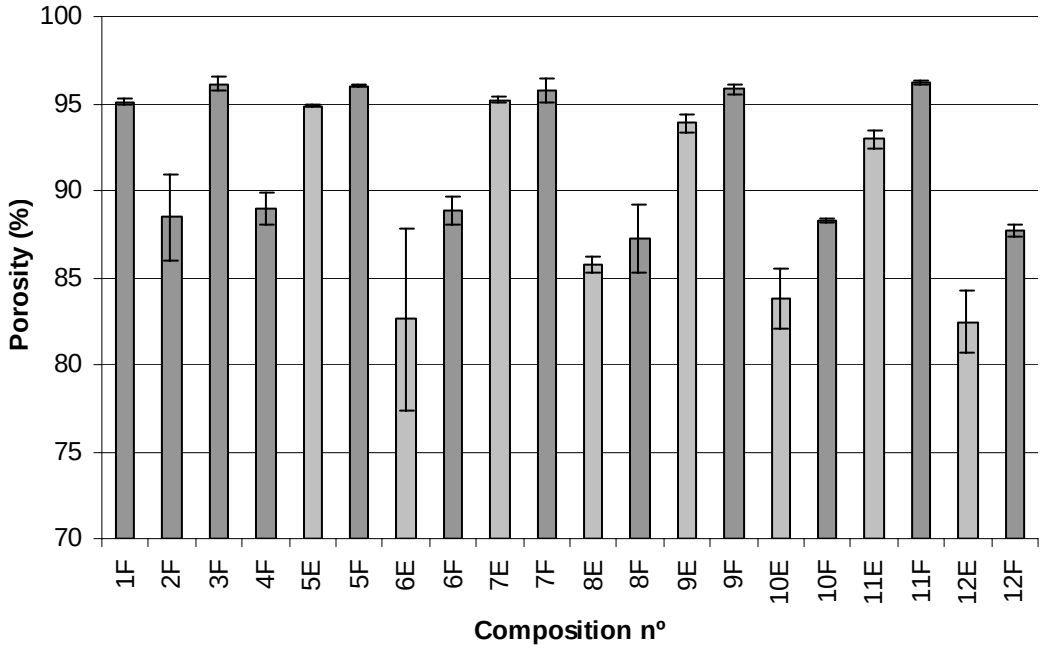

Figure 3.9: Porosity results for compositions 1-12.

Experiment design analysis

The porosity of compositions nº 5-12 was analysed using experiment design analysis. Compositions nº 1-4 were excluded from the analysis due to the handling and heterogeneity problems they presented. For the sake of clarity, the detailed calculations of the factorial experiment design can be seen in Appendix 3. The polynomial parameters have been adjusted according to the model described in the Chapter 2/ Methods/ Factorial Experiment Design, paragraph nº 4.

Two factors and an interaction were found to have a significant effect on the porosity readings: the PLA w/v%, the solvent removal method, and the interaction between the two. The linear model would read as follows:

$$\textbf{\textit{porosity = 90,47 - 4,63×PLA w/v\% + 1,53×Ext/Dry + 0,66 PLA w/v\%×Ext/Dry}} \quad \{2\}$$

where PLA w/v% stands for the weight/volume percent of PLA in the solvent mixture, Ext/Dry stands for the solvent removal method, either freeze-extraction or

freeze-drying, and the values of PLA w/v% and Solvent removal method correspond to the levels shown in Table 3.1.

Thus, the porosity of the scaffolds within this range of factors depends only on the amount of PLA present in the mix and on the solvent removal method. Higher w/v% of PLA reduce the porosity, logically because there is more matter remaining after solvent removal (Figure 3.10). Solvent removal by freeze-drying created higher porosities as opposed to freeze-extraction (Figure 3.11). This may be due to the fact that the ethanol used in the freeze-extraction has a plasticising effect on the PLA and may cause the structure to shrink slightly thus decreasing the porosity[19]. It may also be due to an incomplete removal of the dioxane by the ethanol, which could cause the PLA structure to shrink. The interaction between PLA w/v% and the solvent removal method is illustrated in Figure 3.12; at low PLA w/v% the effect of the solvent removal is much smaller than at high PLA w/v%.

It is interesting to point out that the porosity depends neither on the quenching temperature nor on the presence of water in the mix. This is also the case at low quenching temperatures such as in liquid nitrogen and can been seen from the results of compositions 1-4F in Figure 3.9.

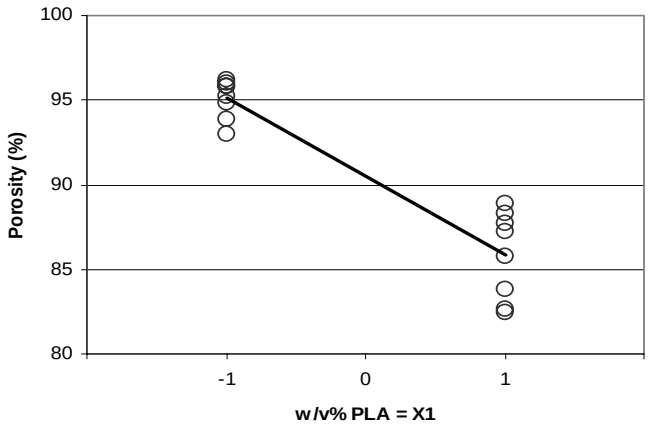

Figure 3.10: Effect of the PLA w/v% (X1) on the porosity of the scaffolds. The line represents the tendency of the average value of the porosity as the value of the PLA w/v% (X1) varies from –1 to +1.

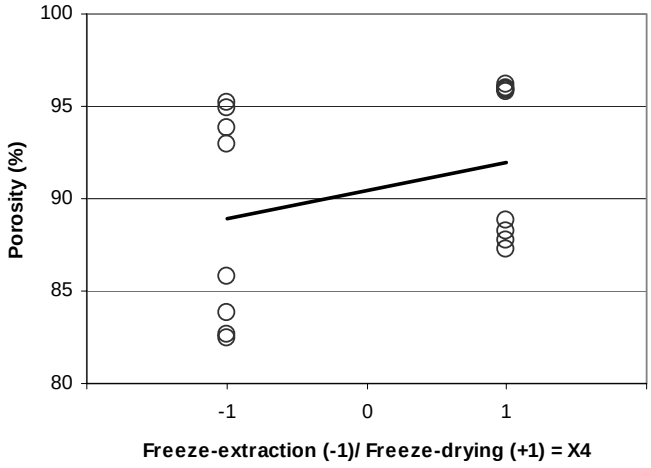

Figure 3.11: Effect of the solvent removal method (X4) on the porosity of the scaffolds. The line represents the tendency of the average value of the porosity as the value of the solvent removal method (X4) varies from –1 to +1.

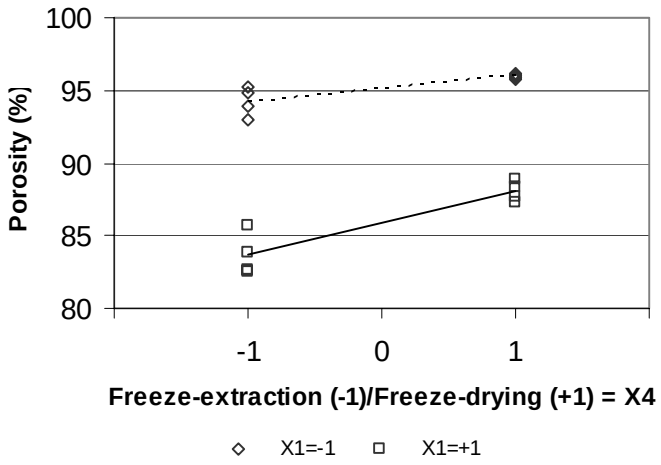

Figure 3.12: Effect of the interaction between the PLA w/v% (X1) and the solvent removal method (X4) on the porosity of the scaffolds. The dotted line represents the tendency of the average value of the porosity as the solvent removal method (X4) varies from –1 to +1 when the PLA w/v% (X1) is -1. The full line represents the tendency of the average value of the porosity as the solvent removal method (X4) varies from –1 to +1 when the PLA w/v% (X1) is +1.

The results of the preliminary study with PLA scaffolds have given a great amount of insight into the nature of the phase-separation method and the effects of the composition and processing conditions on scaffold porosity and morphology. From a

qualitative point of view, the scaffolds had numerous defects in the structure due to the solidification during quenching and the entrapment of air bubbles. The defects due to the solidification are more pronounced on low w/v% PLA scaffolds, and could be reduced by using moulds made of a less conductive material than aluminium which would reduce the temperature gradient within the mix during quenching or by increasing the PLA w/v%. The presence of air bubbles was higher at high PLA w/v%, probably due to the high viscosity of the mix which does not allow the air bubbles to rise. These defects could be reduced by using lower PLA w/v%. Thus, a compromise must be attained between high and low w/v% of PLA in order to reduce quenching defects, avoid air bubble entrapment, and maintain an appropriate porosity. Thus, Teflon moulds were used in the following study on the optimisation of PLA/G5 composite scaffolds, in an attempt to improve the quality of the samples (Figure 3.14). Furthermore, the maximum PLA w/v% was reduced from 7.5% to 6% in order to reduce the number of defects in the scaffolds.

The presence of water in the mix created microporosity within the pore walls, probably due to the phase separation between the PLA and the water after dioxane solidification. This microporosity, which can be clearly seen in the SEM images (Figure 3.5) does not affect the overall porosity.

The quenching temperature had no significant effect on the overall porosity of the samples. In accordance with the literature, quenching at liquid nitrogen temperatures did reduce pore size significantly [13]. This effect is not obvious in compositions nº 5-12 between 0°C and -20°C, perhaps due to the small temperature difference between the levels or to the difficulty in measuring pore size accurately due to the two-dimensional nature of the SEM images and the material's anisotropy. The optimisation study with glass particles did not include liquid nitrogen temperatures due to the poor quality of the scaffolds produced in this manner. Indeed, -196°C is a very severe quenching temperature, and though their microstructure was interesting, they were often cracked and broken macroscopically (Figure 3.13).

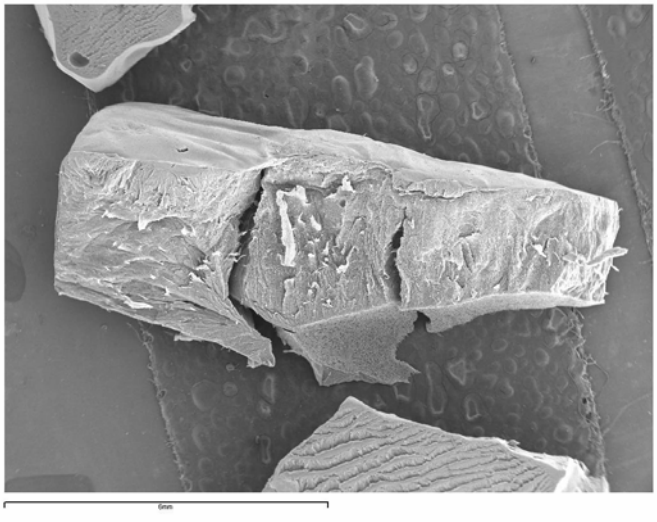

Figure 3.13: SEM image illustrating the poor quality of the scaffolds quenched at liquid nitrogen temperatures: composition 1F is shown in the image. (The magnification bar corresponds to 6mm)

The solvent removal method affected the overall porosity significantly. In effect, removing the dioxane by freeze-extraction reduced the porosity of the scaffolds. This could be due solely to the contact between the PLA and the ethanol, or to the presence of residual dioxane in the scaffolds after solvent removal which could cause shrinkage. In order to elucidate the reason behind the effect of freeze-extraction, its processing protocol was changed for the optimisation experiment. In the following study, the scaffolds were soaked in ethanol during three days, and the ethanol was changed thrice during this time.

Characterisation and optimisation of PLA/G5 glass composite scaffolds

Materials and Methods

Following the preliminary test, the optimum composition and processing of the PLA + Glass scaffolds was endeavoured. The characterisation and optimisation of the composite scaffolds was carried out by means of a 2^4 experimental design. Four aspects of scaffold composition, the four factors, were varied. These factors were: a) quenching temperature, b) w/v% of the PLA/dioxane solution, c) v/v% of water in the 1,4-

dioxane/water solution, and d) solvent removal method: freeze-extraction or freeze-drying. All factors were tested at two levels: a maximum (+1) and a minimum (-1) (Table 3.3, Table 3.4).

All scaffolds contained 50 weight percent (wt%) of G5 glass particles, milled and sieved below 40 microns. Aluminium foil moulds were no longer used in this study due to reproducibility problems. Teflon moulds were designed and manufactured to prepare cylindrical scaffolds measuring 20mm in diameter and 15mm in height. The moulds had stainless steels covers (Figure 3.14).

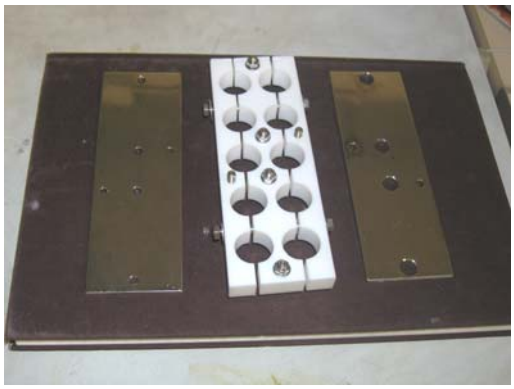

Figure 3.14 : Teflon moulds with stainless steel covers used to manufacture the composite scaffolds

	Quenching Temperature	w/v% of PLA	v/v% of H_2O in the solvent	Solvent removal method
Low level (-1)	-20°C	2%	0%	Freeze-extraction
High level (+1)	0°C	6%	7.5%	Freeze-drying

Table 3.3: Levels of the factors used for the optimisation of the composite scaffolds

Composition Nº	Quenching Temperature	w/v% of PLA	v/v% of H_2O in the solvent	Solvent removal method
J1	-1	-1	-1	-1
J2	+1	-1	-1	-1
J3	-1	+1	-1	-1
J4	+1	+1	-1	-1
J5	-1	-1	+1	-1
J6	+1	-1	+1	-1
J7	-1	+1	+1	-1
J8	+1	+1	+1	-1
J9	-1	-1	-1	+1
J10	+1	-1	-1	+1
J11	-1	+1	-1	+1
J12	+1	+1	-1	+1
J13	-1	-1	+1	+1
J14	+1	-1	+1	+1
J15	-1	+1	+1	+1
J16	+1	+1	+1	+1

Table 3.4: Composition of the 16 samples used for the optimisation of the composite scaffolds

The morphology and porosity of the samples were evaluated as described above. Porosity measurements are presented as an average of five samples. The mechanical properties were measured by compression tests. The thermal properties of the scaffolds and the residual dioxane were also measured.

Mechanical Properties

Compression tests were performed on an Adamel Lhomargy tensile testing machine, with a 100N or 10kN load cell for compositions with 2% or 6% PLA w/v% respectively. A constant crosshead speed of 2mm/min was applied until 50% strain of the sample. All compression samples measured 16mm in diameter and 8mm in height.

(Sample dimensions are smaller than mould dimensions due to shrinkage). The stiffness of the scaffolds is defined as the slope of the initial linear portion of the stress strain curve, the slope was measured at intervals of 0.025 strain (ε) until the difference between the values was more than 10%, starting at ε = 7.5%. Measurements are presented as an average of five samples.

Thermal properties

DSC measurements were carried out on a TA Instruments DSC 2820. Samples were cooled to 10°C and subjected to two heating cycles. During each cycle, samples were heated to 200°C, held isothermally for five minutes and cooled again to 10°C. Both heating and cooling rates were 10°Cmin^{-1}. The heat of fusion, ΔH_f, and the melting temperature, T_m, were recorded during the first cycle in order to determine the crystallinity, X_c. The melting temperature was defined as the minimum of the melting peak. The heat of fusion is defined as the area of the fusion peak. In the case of the composite material, the value of ΔH_f must be corrected to take the weight of the glass phase into account. Thus, the corrected heat of fusion, $\Delta H_{fcorr,}$ is ΔH_f / (wt% of polymer). The crystallinity is then computed as the ratio between the corrected heat of fusion of the sample and the theoretical value of the heat of fusion of a 100% crystalline monodispersed LL-PLA, ΔH_f^0, as reported by Fischer : 93.1 J/g, (see equation {3}) [28]. The glass transition temperature (T_g) was determined during the second cycle as the inflection point of the glass transition (Figure 3.15).

$$\%X_c = \frac{\Delta H_{fcorr}}{\Delta H_f^0} \qquad \{3\}$$

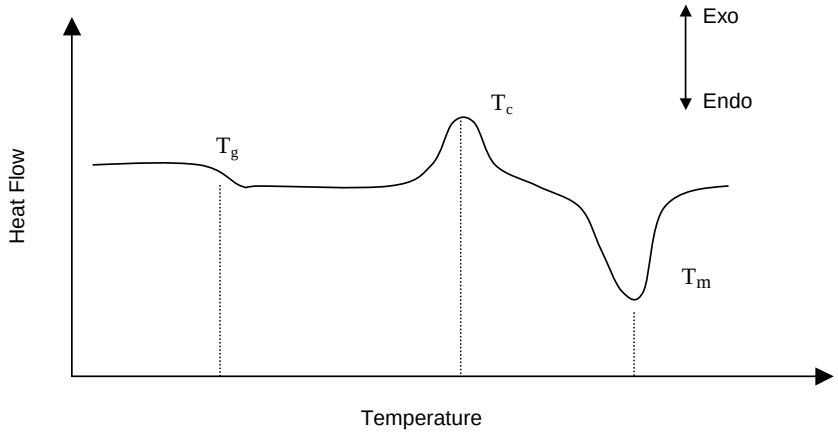

Figure 3.15: Schematic diagram of a heat flow curve showing the glass transition temperature, T_g, the crystallisation temperature, T_c, and the melting point, T_m.

Results and Discussion

Morphology

The general morphology of the scaffolds containing 50 wt% of glass particles was similar to those without glass of the preliminary study. Although some samples still presented cavities due to quenching, fairly regular samples were also attained (Figure 3.16). Despite the use of the Teflon moulds which should be less conductive, the porosity was still highly oriented from the mould walls towards the centre. Measuring the exact pore sizes is not straightforward due to the anisotropy of the porosity but in general macropores seem to be approximately 100μm in diameter.

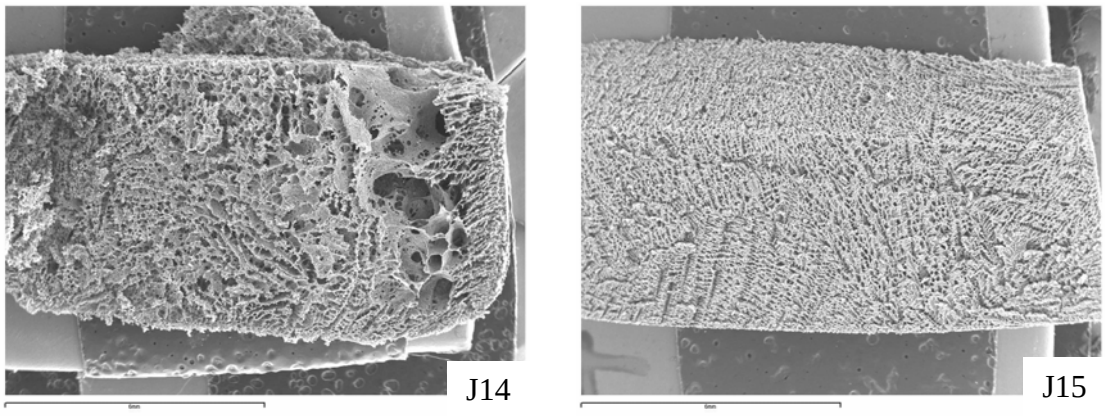

Figure 3.16: SEM images of scaffolds J14 and J15. J14 presented large cavities whereas J15 had no visible defects. (Magnification bars correspond to 6mm)

The effect of the quenching temperature on the pore size is noticeable. Compositions quenched at 0°C have larger pores than those quenched at -20°C. This effect is illustrated in Figure 3.17, in which compositions J3 and J13 are quenched at -20°C; whereas J4 and J14 are quenched at 0°C. This effect had been seen clearly in the previous study on scaffolds quenched at liquid nitrogen temperatures, but was less clear between 0°C and -20°C. This is perhaps due to the nature of the Teflon moulds which allow for a more gradual solidification of the mix.

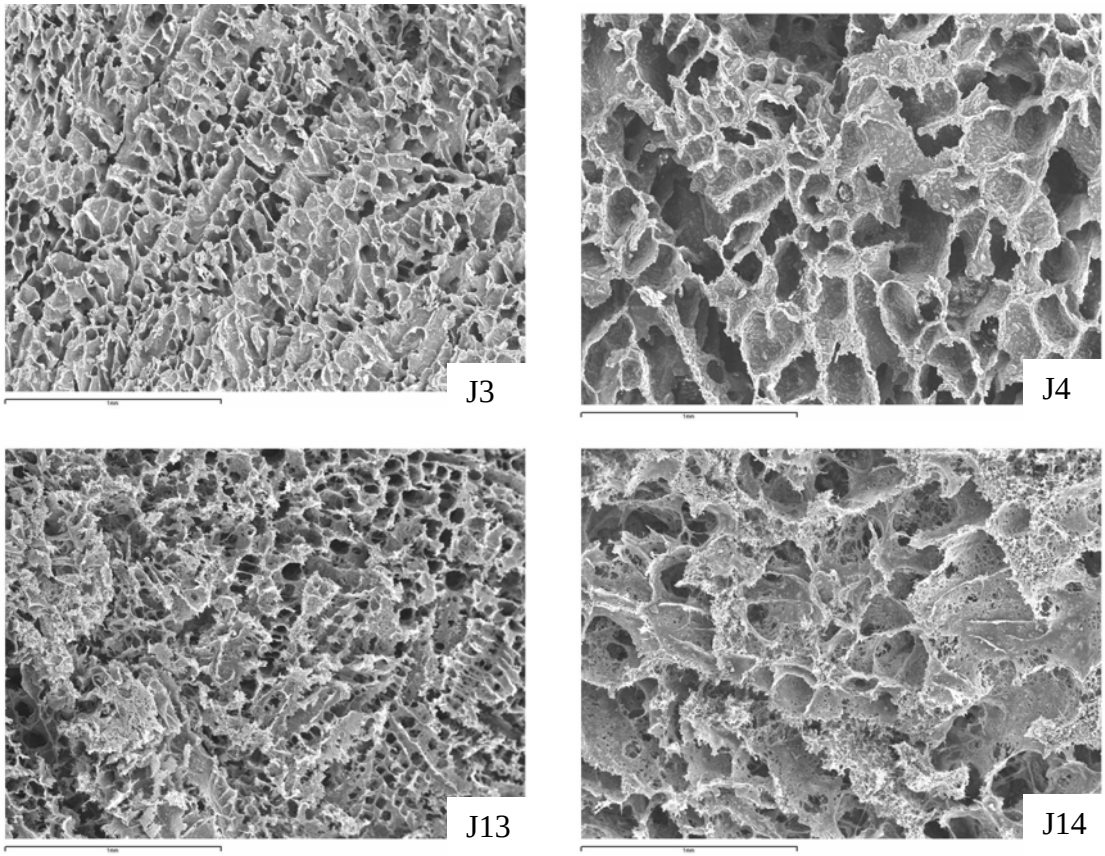

Figure 3.17: SEM images of compositions J3, J4, J13 and J14 illustrating the effect of quenching temperature on pore size. Compositions J3 and J13 are quenched at -20°C whereas compositions J4 and J14 are quenched at 0°C. (Magnification bars correspond to 1mm)

The presence of water in the mix created microporosity within the pore walls as was the case in the preliminary study. It also affected the binding of the glass particles within the polymer matrix. As can be seen in Figure 3.18, compositions J4 and J11, which do not contain H_2O, present very solid pore walls with tightly bound glass particles. The glass particles are in effect completely coated by the PLA. In the case of compositions J8 and J15, which do contain H_2O, the glass particles seem to lie loosely within the microporosity of the pore walls. As is often cited in the literature, the presence of water seems to induce a liquid-liquid spinodal decomposition, the typical spinodal morphology can be seen at high magnifications (Figure 3.19).

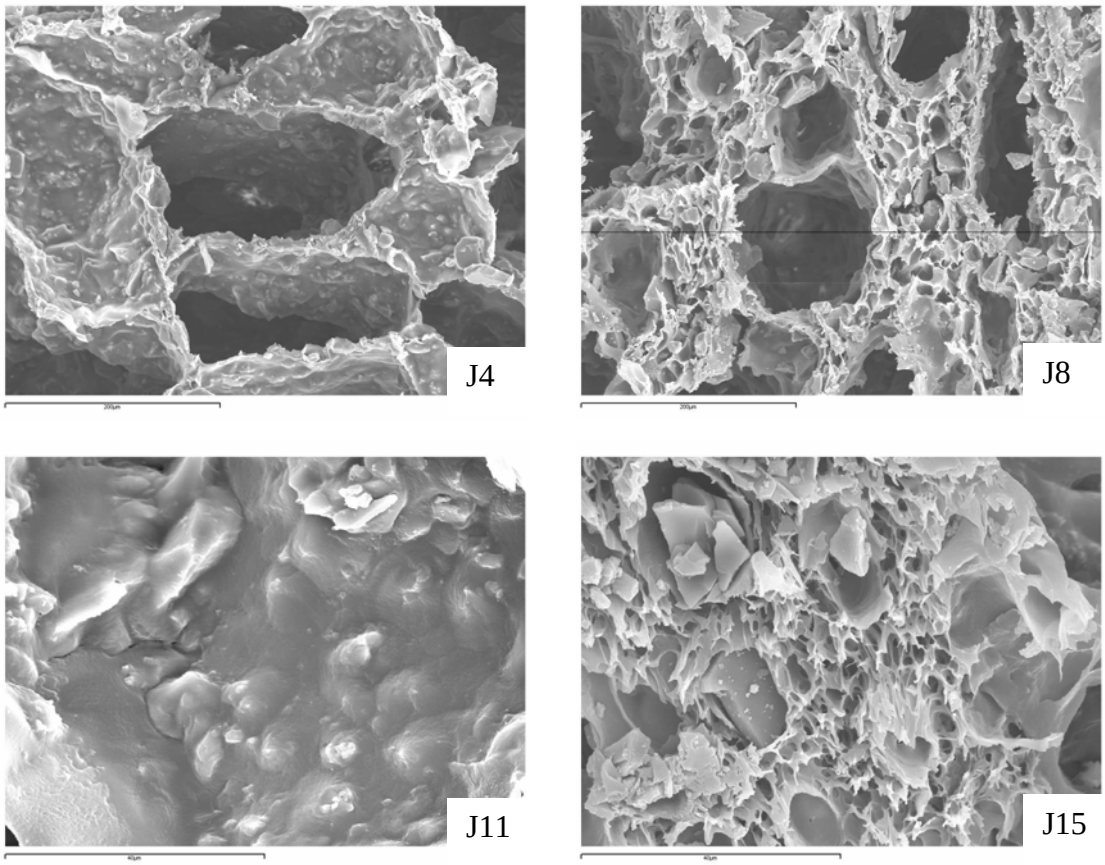

Figure 3.18: SEM images of compositions J4, J8, J11 and J15 illustrating the effect of H_2O on the morphology of the scaffolds. Images of J8 and J15 show the microporosity which is created within the pore walls, and the loose attachment of the glass particle within the polymer matrix. The images of J4 and J11 show solid pore walls and glass particles which are intimately bound within the polymer matrix. (Magnification bars correspond to 40μm)

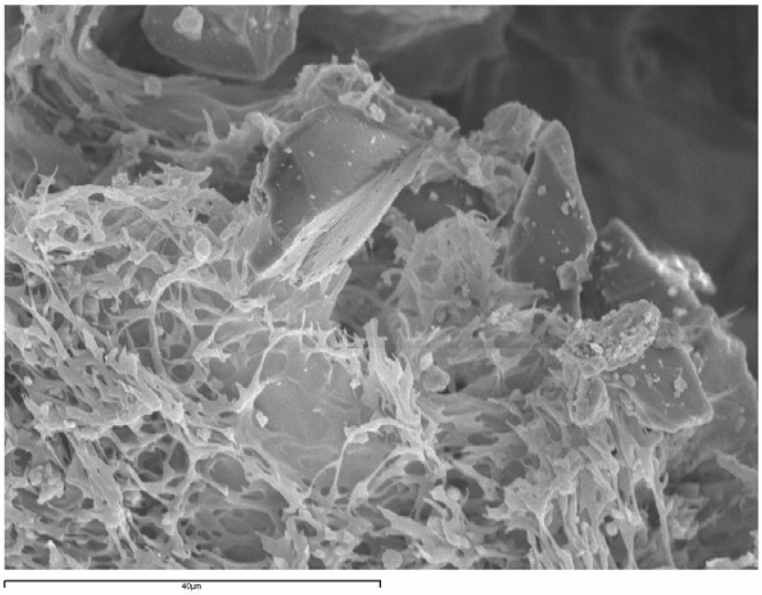

Figure 3.19: SEM image of composition J2 illustrating the typical spinodal decomposition morphology of the PLA surrounding the glass particles. (Magnification bar corresponds to 40μm)

The w/v% of PLA in the scaffolds affected the pore shape and the organisation of scaffolds morphology. Low PLA w/v% seemed to create "fluffy" highly porous scaffolds. High PLA w/v%, on the other hand, create solid oriented pore networks. This effect seems to be enhanced by the presence of water (Figure 3.20).

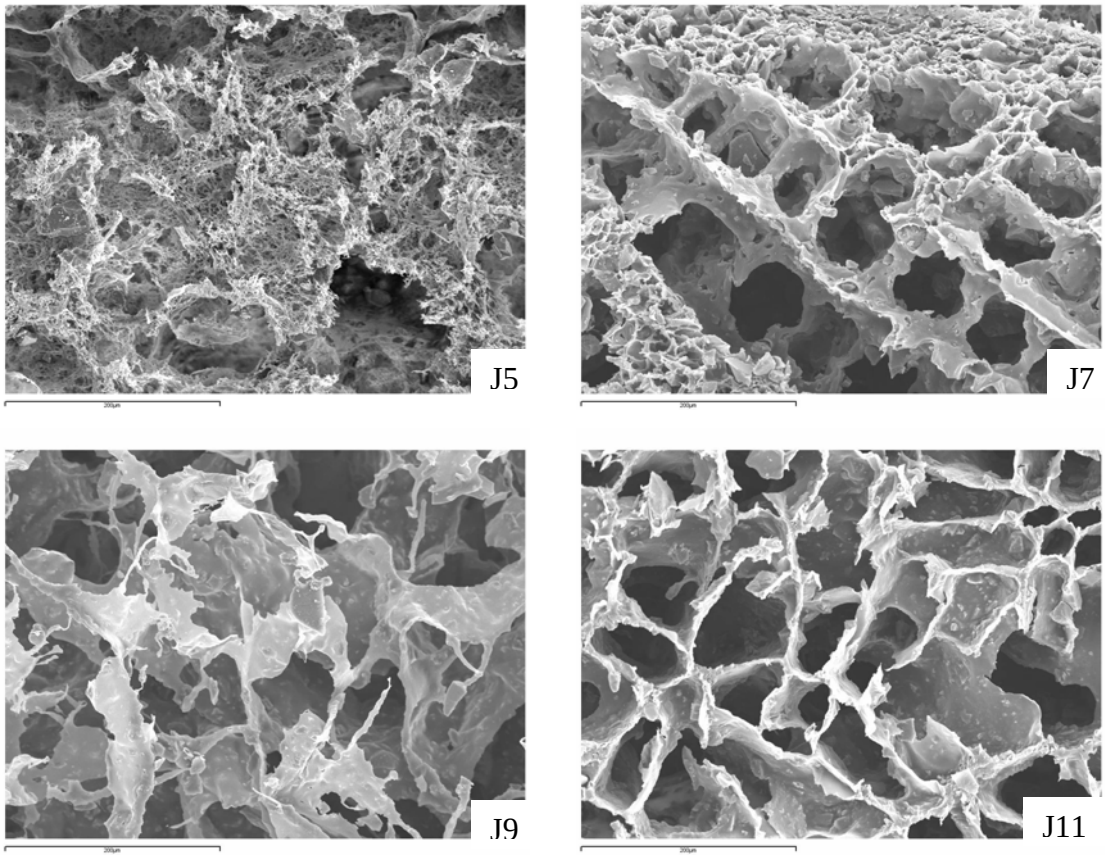

Figure 3.20: SEM images illustrating the effect of PLA w/v% on the morphology of the scaffolds. At low PLA w/v% (compositions J5 and J9), scaffold morphology is more porous and less organised. At high PLA w/v% (compositions J7 and J11), scaffold morphology is highly oriented and pore walls are thicker. (Magnification bar corresponds to 200μm)

Factor	Qualitative effect
Quenching Temperature	▪ The lower the quenching temperature the smaller the pore size
Presence of H_2O in the solvent	▪ Presence of microporosity within pore walls ▪ Spinodal decomposition morphology
PLA w/v%	▪ Low PLA w/v% create a "fluffy" highly porous morphology (this effect is enhanced in the presence of H_2O)

Table 3.5: Summary of the effects of the factors of the experiment design analysis, on the morphology of the scaffolds.

Porosity

The porosity results for composition J1-J16 can be seen in Figure 3.21. The porosity ranges between 86% and 96%. These porosities were analysed using experiment design analysis. For the sake of clarity, the detailed calculation can be seen in Appendix Chapter 3. Only one factor was found to have a significant effect on scaffold porosity: the PLA w/v%. The linear model would read as follows:

$$\textbf{\textit{porosity = 91.2- 4,005×PLA w/v\%}} \quad \{4\}$$

where PLA w/v% stands for the weight/volume percent of PLA in the solvent mixture, and the values of PLA w/v% correspond to the levels shown in Table 3.1.

Unlike in the preliminary study, the solvent removal method is no longer significant. Thus the reduction in porosity by freeze-extraction was probably due to an incomplete removal of the dioxane. Increasing the soaking time and refreshing the ethanol made the freeze-extraction method equivalent to freeze-drying in terms of porosity. It is also interesting to note that the linear model is similar to that of the preliminary study (equation {2}). Similar studies in the literature agree with this study, and find no influence of the v/v% of H_2O nor the quenching temperature on the overall porosity of the scaffolds [13].

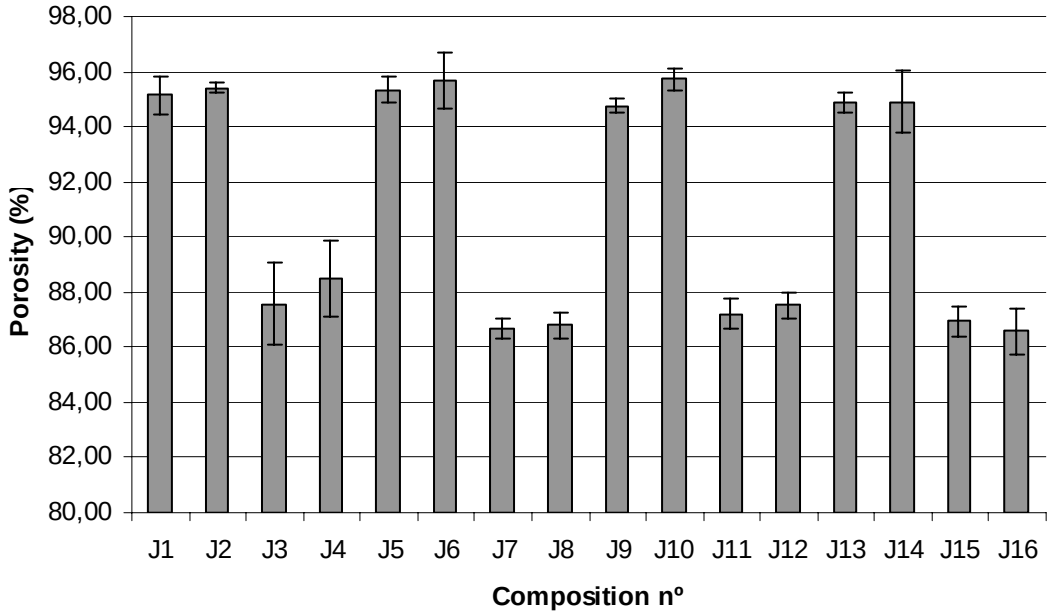

Figure 3.21: Porosity results for compositions J1-J16

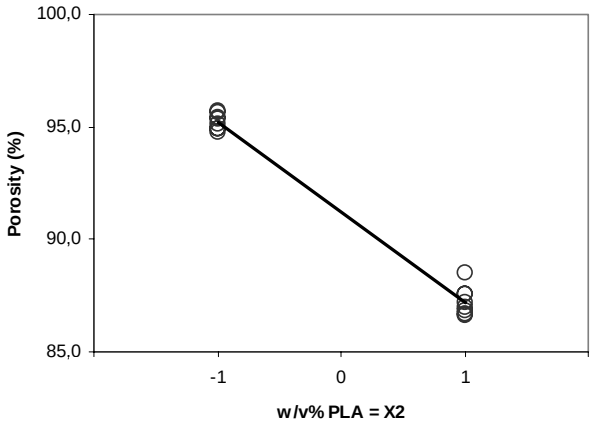

Figure 3.22: Effect of the w/v% of PLA on the porosity of the scaffolds. The line represents the tendency of the average value of the porosity as the value of the PLA w/v% (X2) varies from –1 to +1.

Mechanical Properties

The mechanical properties of the scaffolds were evaluated by performing compression tests. The results can be seen in Figure 3.23. (The numerical values can be seen in the Appendix Chapter 3). The stiffness of the scaffolds varies between 0.29 MPa

and 10 MPa. Compositions with low PLA w/v% have stiffnesses which are practically an order of magnitude smaller than those with high PLA w/v%.

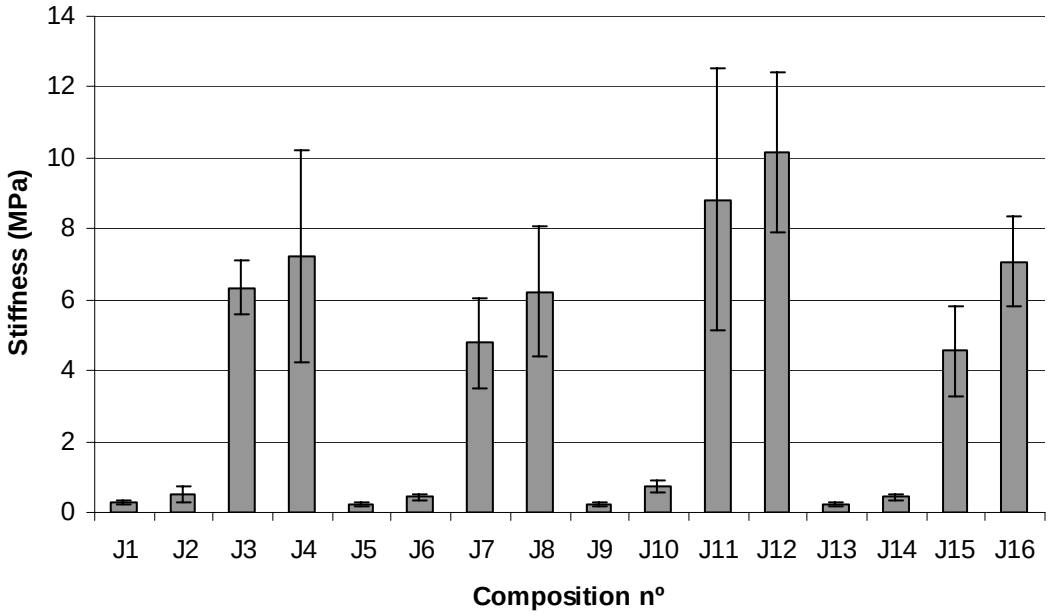

Figure 3.23: Compression test results for compositions nº J1-J16

The results were analysed using experiment design analysis. For the sake of clarity, the detailed calculation can be seen in the Appendix Chapter 3. Three factors and an interaction were found to have a significant effect on scaffold stiffness: PLA w/v%, the quenching temperature and the v/v% of H_2O in the mix. The interaction between the w/v% of PLA and the v/v% of H_2O was also significant. The influence of the PLA w/v% is much larger than that of the other factors; this can be seen by the magnitude of its corresponding β. The linear model would read as follows:

$$\textit{Stiffness} = 3.64 + 3.527 \times \textit{PLA w/v\%} - 0.65 \times \textit{v/v\% } H_2O + 0{,}46\ \textit{Quench. T} - 0.59 \times \textit{PLA w/v\%} \times \textit{v/v\% } H_2O \quad \{5\}$$

where PLA w/v% stands for the weight/volume percent of PLA in the solvent mixture, v/v% H_2O stands for the volume/volume percent of H_2O in the solvent

mixture, Quench.T. stands for the quenching temperature and all values correspond to the levels shown in Table 3.1.

The most important effect is that of PLA w/v% which increases the stiffness of the scaffolds by an order of magnitude (Figure 3.24). This is certainly related to the reduction of the porosity mentioned above. The negative effect of H_2O on scaffold properties could be due to the microporosity it produces within the pore walls which may make them weaker (Figure 3.25), or the fact that the glass particle are not as tightly bound by the PLA matrix. The effect of water, however, interacts with the PLA w/v%. It is negative at high PLA w/v% and practically null at low PLA w/v% (Figure 3.25), thus high PLA w/v% reinforce the detrimental effect of H_2O on the stiffness of the scaffolds. Finally higher quenching temperatures increase scaffold stiffness, perhaps due to the larger pore sizes and thus thicker pore walls (Figure 3.26).

It is interesting to note the considerable compressive moduli of the scaffolds. Maquet et al.[15;20] and Ma and Zhang [21] report moduli of 10-20 MPa and approximately 10MPa respectively. These moduli are certainly higher than those obtained in solvent casting procedures[22-24], which range between 100 and 500 kPa. Although the porosities of the phase-separated scaffolds are lower, those with interesting mechanical properties have porosities ranging between 86% and 88%, which is acceptable for tissue engineering applications. Furthermore, the solvent extraction method guarantees the permeability and interconnectivity of the porosity, which is a basic criteria for tissue engineering scaffolds[8;25].

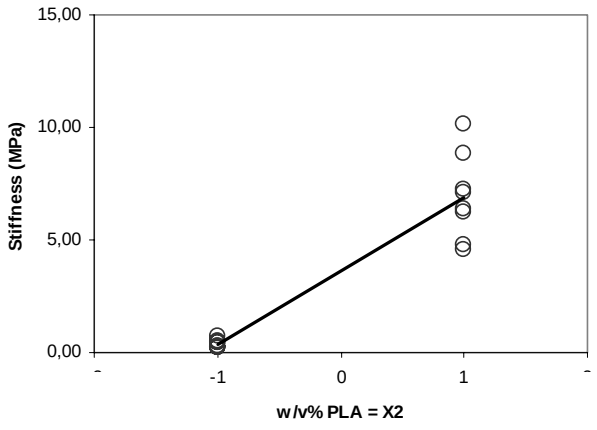

Figure 3.24: Effect of the PLA w/v% (X2) on the stiffness of the scaffolds. The line represents the tendency of the average value of the stiffness as the value of the PLA w/v% (X2) varies from –1 to +1.

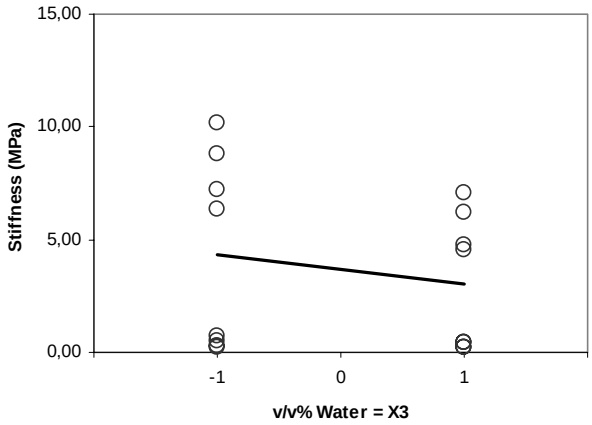

Figure 3.25: Effect of the v/v% of H_2O on the stiffness of the scaffolds. The line represents the tendency of the average value of the stiffness as the value of the H_2O v/v% (X3) varies from –1 to +1.

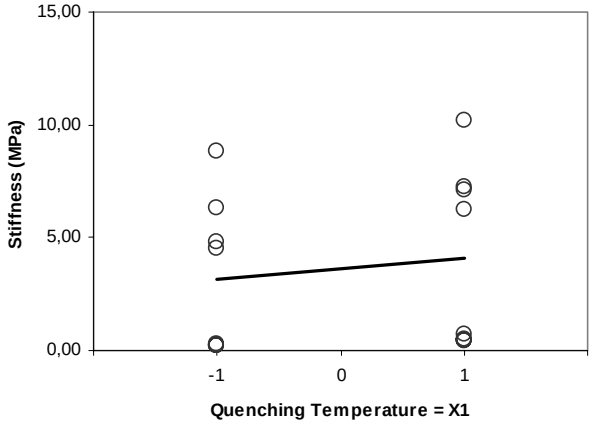

Figure 3.26: Effect of the quenching temperature (X1) on the stiffness of the scaffolds. The line represents the tendency of the average value of the stiffness as the value of the quenching temperature (X1) varies from –1 to +1.

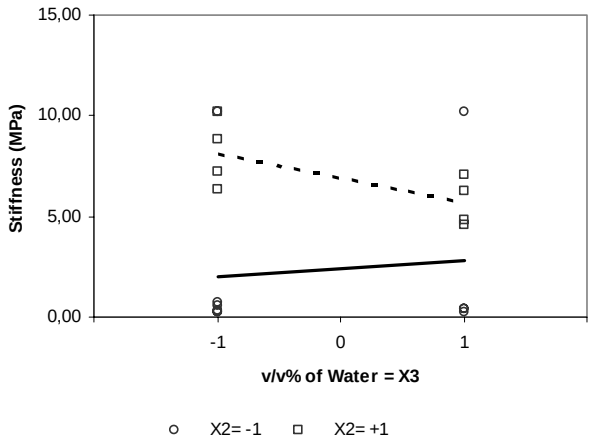

Figure 3.27: Effect of the interaction between the PLA w/v% (X2) and the H_2O v/v% (X3) on the stiffness of the scaffolds. The dotted line represents the tendency of the average value of the stiffness as the v/v% of H_2O (X3) varies from –1 to +1 when the PLA w/v% (X2) is -1. The full line represents the tendency of the average value of the stiffness as the v/v% of H_2O (X3) varies from –1 to +1 when the PLA w/v% (X2) is +1.

Thermal Properties

Crystallinity

DSC measurements were used to compute the values of crystallinity and Tg for compositions J1-J16. The crystallinity results for compositions J1-J16 can be seen in Figure 3.28. The results were analysed using experiment design analysis. For the sake of clarity, the detailed calculation can be seen in Appendix Chapter 3.

Two factors and two interactions were found to have a significant effect on the crystallinity of the scaffolds: the quenching temperature, the v/v% of H_2O in the solvent, the interaction between the two and the interaction between the quenching temperature and the w/v% of PLA. The linear model would read as follows:

$$\textbf{\textit{Crystallinity} = 29.7 + 5.4×Quench.T. + 4.6×}H_2O\textbf{ v/v\% + 3.6×Quench.T×}H_2O\textbf{ v/v\% - 3.0×Quench.T. ×PLA w/v\%} \quad \{6\}$$

where Quench.T. stands for quenching temperature, H_2O v/v% stands for the volume/volume percent of H_2O in the solvent, PLA w/v% stands for the weight/volume percent of PLA in the solvent mixture, and all values correspond to the levels shown in Table 3.1.

High quenching temperatures increase the crystallinity of the polymer (Figure 3.29). This is due to the milder quenching induced by the smaller temperature gradient. At low quenching rates, the polymer chains have more time to arrange into crystals.

The presence of H_2O in the solvent mixture also increases the crystallinity of the polymer (Figure 3.30) and this effect is much more pronounced at high quenching temperatures (Figure 3.31). This effect has been reported in the literature and is related to the nature of the phase separation, i.e. liquid-liquid phase separation with the occurrence of gelation [1;8;13;26]. In effect, the presence of water in the mix promotes liquid-liquid phase separation, and may give rise to spinodal decompositions, as was discussed in the section on morphology and illustrated in Figure 3.19. Schugens et al.[1] study the phase separation of polylactide solutions in 1,4-dioxane as a function of the polymer crystallinity, molecular weight and concentration. In their study, gelation is only observed at low quenching rates and in the presence of H_2O. Gelation occurs through the formation of microcrystalline domains that act as cross-links. The gel is stabilised by a continuous polymer-rich phase in which the polymer chains are cross-linked by local crystallisation. Regarding compositions J1-J16, SEM images and crystallinity readings seem to indicate that a liquid-liquid phase separation is taking place in the presence of H_2O. The occurrence of gelation would explain why the presence of H_2O and its interaction with the quenching rate enhances the crystallinity of the polymers.

Finally, low polymer concentrations combined with high quenching temperatures have been found to enhance the crystallinity of phase-separated scaffolds (Figure 3.32). Numerous studies have shown that low polymer concentrations favour higher crystallinity. This is due to the fact that solutions are more dilute, therefore less viscous and the polymer chains can move more freely. In the case of this study, the effect of low quenching rates is enhanced by low polymer concentrations[27].

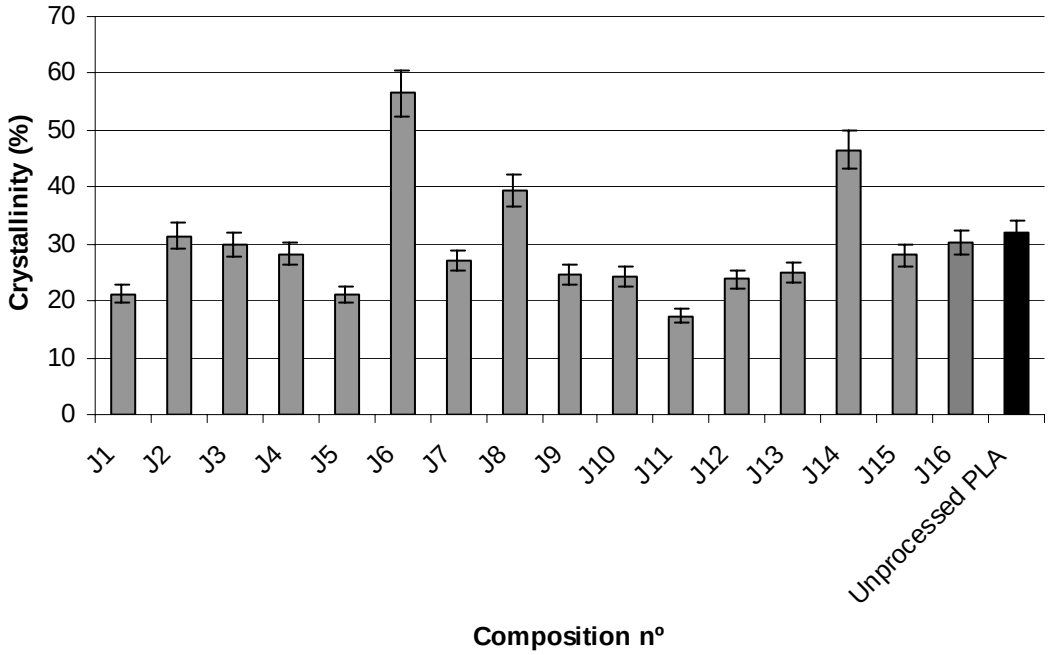

Figure 3.28: Crystallinity results for compositions J1-J16

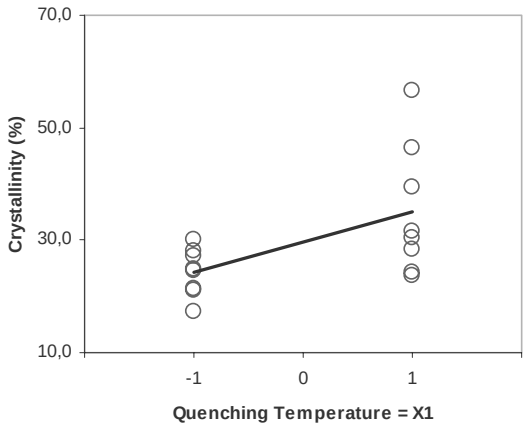

Figure 3.29: Effect of the quenching temperature (X1) on the crystallinity of the scaffolds. The line represents the tendency of the average value of the crystallinity as the value of the quenching temperature (X1) varies from –1 to +1.

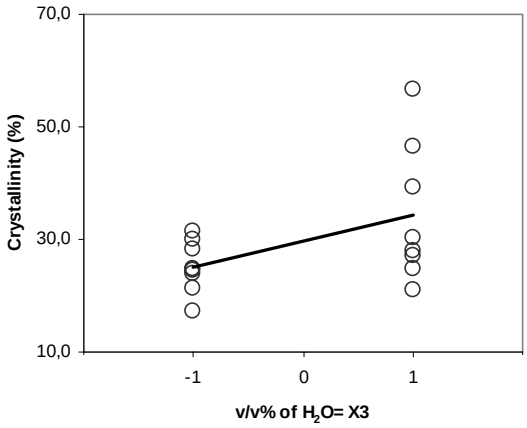

Figure 3.30: Effect of the v/v% H2O (X3) on the crystallinity of the scaffolds**.** The line represents the tendency of the average value of the crystallinity as the value of the v/v% of H_2O (X3) varies from –1 to +1.

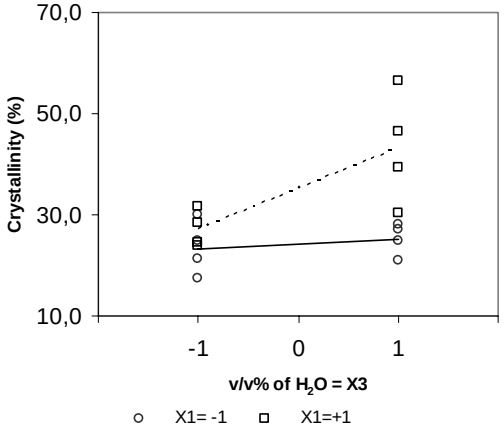

Figure 3.31: Effect of the interaction between the v/v% of H_2O (X3) and the quenching temperature (X1). The dotted line represents the tendency of the average value of the crystallinity as the v/v% of H_2O (X3) varies from –1 to +1 when the Quenching Temperature (X1) is -1. The full line represents the tendency of the average value of the crystallinity as the v/v% of H_2O (X3) varies from –1 to +1 when the Quenching Temperature (X1) is +1.

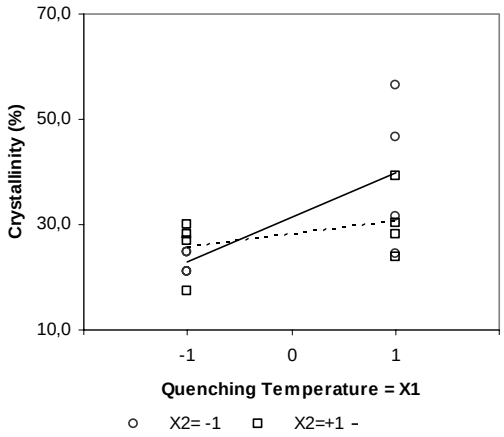

Figure 3.32: Effect of the interaction between the quenching temperature (X1) and the w/v% of PLA (X2). The dotted line represents the tendency of the average value of the crystallinity as the Quenching Temperature (X1) varies from –1 to +1 when the w/v% of PLA (X2) is +1. The full line represents the tendency of the average value of the crystallinity as the Quenching Temperature (X1) varies from –1 to +1 when the w/v% of PLA (X2) is -1.

Glass Transition Temperature (Tg)

The Tg readings for compositions J1-J16 can be seen in (Figure 3.33). It is clear that compositions J9-J16 have a higher and more constant Tg than compositions J1-J8. Compositions J9-J16 are all processed by freeze-drying, whereas the others are processed by freeze-extraction. In effect the experiment design analysis reveals that the solvent extraction method is the key factor which influences scaffold Tg. The other factors are the PLA w/v% and the interaction between the two (detailed calculations can be seen in Appendix Chapter 3).

The linear model would read as follows:

$$Tg = 57{,}82 + 3{,}848 \times Ext/Dry - 1{,}578 \times Ext/Dry \times PLA\ w/v\% + 1{,}468 \times PLA\ w/v\% \quad \{7\}$$

Where Ext/Dry stands for the solvent extraction method, PLA w/v% stands for the weight/volume percent of PLA in the polymer/solvent mix, and all values correspond to the levels shown in Table 3.1.

The effect of the solvent extraction method is probably due to the effect of the ethanol. Solvent removal by freeze-drying involves practically the same conditions as during quenching (-20°C), plus low pressures, thus no further changes in polymer structure should be expected. Solvent removal by freeze-extraction on the other hand, involves soaking the scaffolds in ethanol for three days. Ethanol molecules may have a plasticising effect on the PLA structure, provoking polymer chain scission and thus reducing the Tg. The effect of the ethanol on the PLA was previously noted in the preliminary study. The significance of the interaction between the solvent extraction method and the PLA w/v% implies that the plasticising effect is reinforced at low PLA concentrations. This is probably due to the higher porosity (Figure 3.22) and thus higher surface area in contact with the ethanol. The effect of PLA w/v% alone is positive, thus Tg increases at higher PLA w/v% (Figure 3.36).

It is interesting to note that the solvent extraction method had no effect on the crystallinity of the PLA, thus the ethanol must only affect the amorphous regions of the PLA.

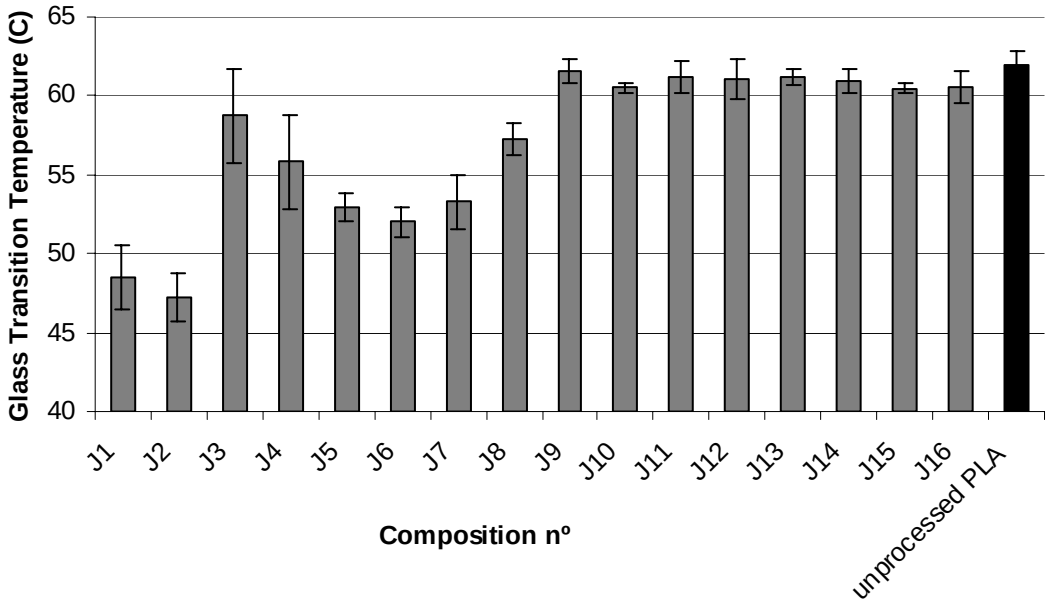

Figure 3.33: Tg results for compositions J1-J16

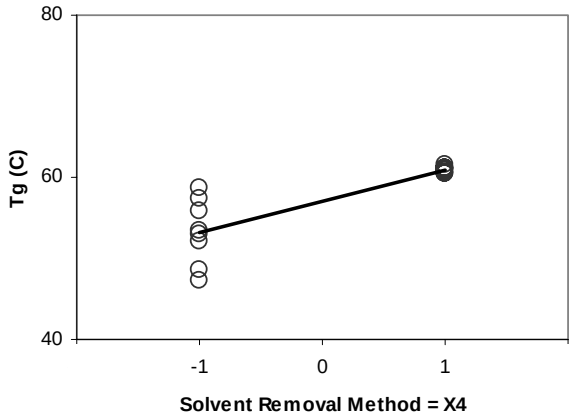

Figure 3.34: Effect of the solvent removal method (X4 = -1 corresponds to freeze-extraction, X4 = 1 corresponds to freeze-drying) on the Tg of the scaffolds. The line represents the tendency of the average value of the Tg as the value of the solvent removal method (X4) varies from –1 to +1.

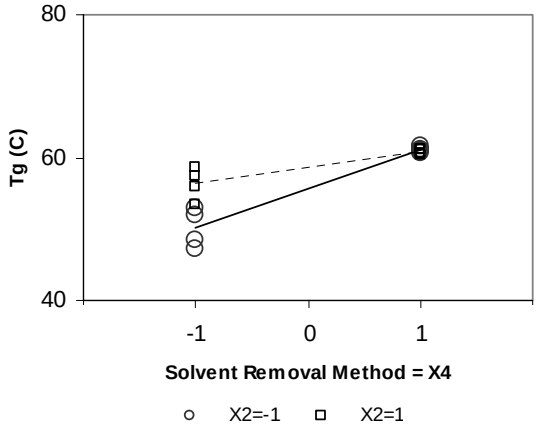

Figure 3.35: Effect of the interaction between the solvent removal method (X4) and the PLA w/v% (X2). The dotted line represents the tendency of the average value of the Tg as the value of the solvent removal method (X4) varies from –1 to +1 when the PLA w/v% (X2) is -1. The full line represents the tendency of the average value of the Tg as the solvent removal method (X4) varies from –1 to +1 when the PLA w/v% (X2) is +1.

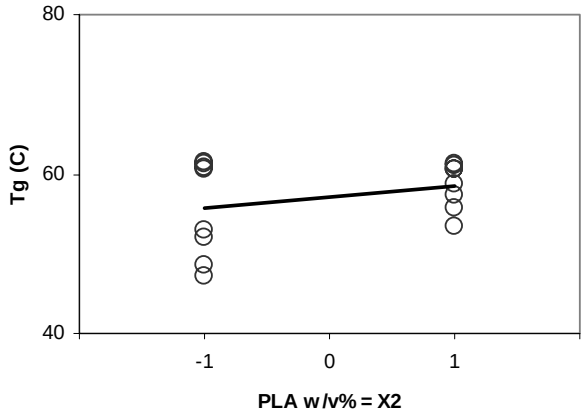

Figure 3.36: Effect of the PLA w/v% (X2) on the Tg of the scaffolds. The line represents the tendency of the average value of the Tg as the value of the PLA w/v% (X2) varies from –1 to +1.

Summary

The results of the characterisation and optimisation study of the composite scaffolds (with glass particles) have revealed further information on the phase-separation method and its effect on the composite material. From a qualitative point of view, the use of Teflon moulds reduced the presence of defects and cavities in the structures and created a more uniform porosity in which changes in pore size due to quenching temperature were obvious (Figure 3.17). Again, as was the case for pure PLA, the presence of H_2O in the solution created microporosity within the pore walls which reduced the coating of the glass particles within the polymer matrix. Furthermore, H_2O produced typical liquid-liquid phase separation morphologies as has been reported in the literature.

Processing by freeze-extraction in ethanol has an interesting effect on the PLA Tg; it lowers the Tg of the scaffolds significantly and also affects its scattering. The scattering is probably due to the fact that the exact time spent in ethanol and the proportion of ethanol to scaffold volume was not surveyed rigorously due to lack of calendar flexibility and storage space.

The stiffness and porosity of the phase-separated composite scaffolds can thus be modulated and optimised by adjusting the composition and the processing parameters of the scaffolds (Table 3.6).

	Quenching T (°C)	w/v% of PLA	v/v % of H_2O in the solvent	Solvent removal method
Porosity		↓		
Stiffness	↑	↑*	↓*	
Crystallinity	↑*	*	↑*	
Tg		↑*		↑*

Table 3.6: Factors of scaffold composition that had a significant effect on the porosity, stiffness, crystallinity and Tg of the scaffolds. ↑ stands for a positive effect, ↓ stands for a negative effect, and * stands for an interaction.

The compositions of the scaffolds used in further studies was determined by the results of this study. Scaffolds with 6% PLA w/v% have optimum stiffnesses taking into account that their porosity is also relatively high. Stiffnesses of 5-10MPa are indeed high for porous tissue engineering scaffolds. The presence of H_2O in the mix was maintained in further studies due to its effect on glass particle binding. In effect the glass particles should play an important role in scaffold chemical and biological behaviour, if they are too tightly coated with polymer, their chemical effect could be compromised or effaced.

In the final compositions, the quenching temperature was fixed at -20°C due to simpler laboratory processing and given the fact that pore sizes and stiffnesses were adequate at both levels. The solvent extraction method was established as freeze-extraction, as was the case with the quenching temperature, it also offered simpler laboratory processing.. Although freeze-extraction was seen to influence scaffold Tg, it did not influence porosity nor stiffness which are critical parameters. The levels of these parameters correspond to composition nº J7 (Table 3.7).

Composition nº	Quenching T (°C)	w/v% of PLA	v/v % of H_2O in the solvent	Solvent removal method
J7	-20°C	6%	7.5%	Freeze-extraction in ethanol

Table 3.7: Detailed composition of J7, the composition with optimum properties and processing parameters

Following studies were pursued with scaffolds containing 5 w/v% of PLA. A PLA w/v% of 5 was chosen (instead of 6% as in this study) in order to increase the porosity of the scaffolds and also for sake of comparison with the solvent cast scaffolds which are produced at 5 w/v% in chloroform.

Effect of glass particles on scaffold properties

Once the composition of the phase-separated scaffolds was determined, a complementary study was performed in order to ascertain the effect of the glass particles on the scaffold properties. Scaffolds were made with pure PLA (5w/v% of PLA), and PLA + G5 glass (50wt% each). The porosity, stiffness and thermal properties of the scaffolds were measured using the methods described above.

The statistical significance of the differences between the averages of the results for all parameters studied was calculated using ANOVA tables with a Fisher multiple comparison test. Statistical significance was established at $p < 0.05$. These calculations have been performed with MINTAB^{TM} Release 14 Minitab Inc. software. When the differences between the values are not statistically significant, they are indicated with a horizontal line in the graphs.

The addition of glass particle in the phase separated scaffolds decreases their porosity significantly (Figure 3.37). Unlike the case of the solvent cast scaffolds, in

which the glass particles tended to weaken the structure, the phase-separated scaffolds' stiffness is reinforced by the addition of 50wt% of glass particles (Figure 3.38).

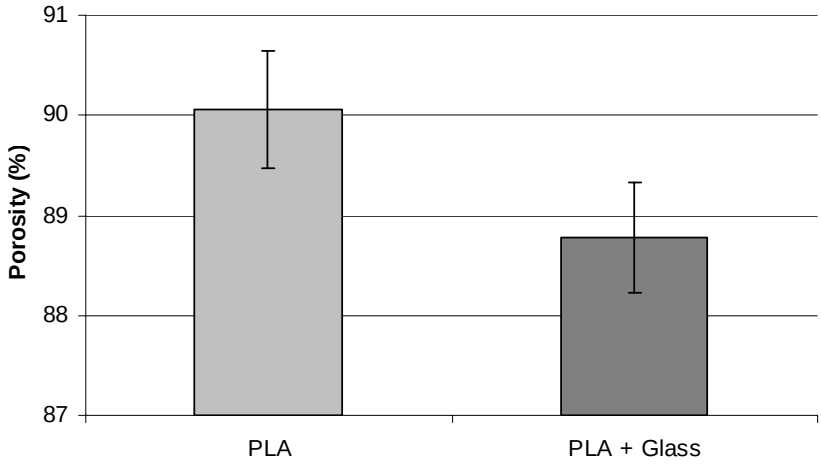

Figure 3.37: Comparison between the porosity of the scaffolds with and without glass particles

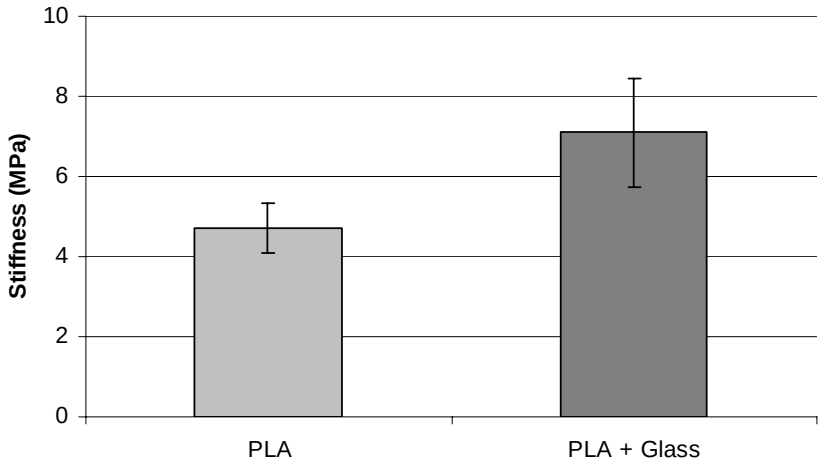

Figure 3.38: Comparison between the stiffness of the scaffolds with and without glass particles

The DSC readings, however, reveal no significant differences between the Tg, Tm and Tc of scaffolds with and without glass particles (Figure 3.39). The addition of glass particles does affect the percentage crystallinity though, making it decrease from 35% to 27% with and without glass respectively (Figure 3.40).

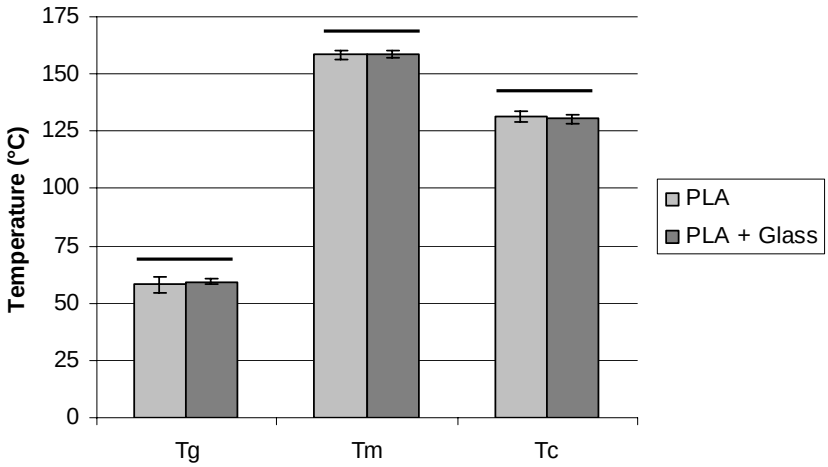

Figure 3.39: Comparison between the Glass Transition Temperature (Tg), melting point (Tm), and crystallisation temperature (Tc) of the scaffolds with and without glass particles. The differences between the scaffolds with and without glass are not statistically significant.

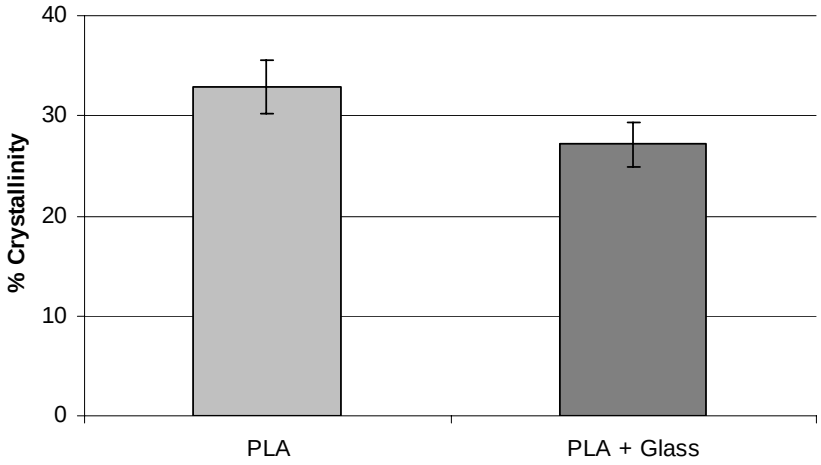

Figure 3.40: Comparison between the percentage crystallinity of the scaffolds with and without glass particles

Conclusions

- SEM images reveal the effect of processing parameters on the morphology of phase-separated scaffolds. PLA w/v% influences the overall porosity, and quenching temperature and the H_2O v/v% influences the nature and size of the pores.
- H_2O v/v% also influences the binding of the glass particles within the PLA matrix and induces liquid-liquid phase separation by spinodal decomposition
- The stiffness of the scaffolds is mainly influenced by their porosity which is in turn solely determined by the PLA w/v%. Scaffolds with low PLA w/v% can attain stiffnesses of 10MPa, which is close to the stiffness of trabecular bone (see Introduction)
- The crystallinity of the PLA in the scaffolds is strongly influenced by the quenching temperature, H_2O v/v% and the w/v% of PLA.
- The soaking of the scaffolds in ethanol in order to extract the dioxane influences the PLA Tg due to the plasticising effect of the ethanol molecules
- The addition of glass particles reinforces the stiffness of the phase-separated scaffolds. It also reduces the porosity slightly, and has no significant effect on their characteristic temperatures: Tg, Tm, Tc
- Scaffolds with low PLA w/v%, and H_2O in the solvent mix were chosen to continue the characterisation due to their good mechanical properties, and to the exposure of the glass particles in the structure.

Publications

The results of this study have been published in:

"Development of biodegradable composite scaffolds for bone tissue engineering: physicochemical, topographical, mechanical, degradation and biological properties"
M.Navarro, C. Aparicio, M.Charles-Harris, E.Engel, M.P.Ginebra, J.A.Planell
Advances in Polymer Science 2006; vol 200, pp 209-215

Bibliography

(1) Schugens C, Maquet V, Grandfils C, Jerome R, Teyssie P. Polylactide macroporous biodegradable implants for cell transplantation. II. Preparation of polylactide foams by liquid-liquid phase separation. J Biomed Mater Res 1996; 30(4):449-461.

(2) Schugens C, Maquet V, Grandfils C, Jerome R, Teyssie P. Bidoegradable and macroporous polylactide implants for cell transplantation: 1. Preparation of macroporous polylactide supports by solid-liquid phase separation. Polymer 1996; 37(6):1027-1038.

(3) Roether JA, Boccaccini AR, Hench LL, Maquet V, Gautier S, Jérôme R. Development and in vitro characterisation of novel bioresorbable and bioactive composite materials based on polylactide foams and Bioglass for tissue engineering applications. Biomaterials 2002; 23:3871-3878.

(4) Zhang Y, Zhang M. Synthesis and characterization of macroporous chitosan/calcium phosphate composite scaffolds for tissue engineering. J Biomed Mater Res 2001; 55:304-312.

(5) Ciapetti G, Ambrosio L, Savarino L, Granchi D, Cenni E, Baldini N, Pagani S, Guizzardi S, Causa F, Giunti A. Osteoblast growth and function in porous poly epsilon -caprolactone matrices for bone repair: a preliminary study. Biomaterials 2003; 24(21):3815-3824.

(6) Zhang R, Ma PX. Poly(α-hydroxyl acids)/hydroxyapatite porous composites for bone tissue engineering. I. Preparation and morphology. Journal of Biomedical Materials Research 1999; 44:446-455.

(7) Ma PX, Zhang R. Synthetic nano-scale fibrous extracellular matrix. J Biomed Mater Res 1999; 46(1):60-72.

(8) Zhang R, Ma PX. Processing of Polymer Scaffolds: Phase Separation. In: Atala A, Lanza RP, editors. Methods of Tissue Engineering. San Diego, San Francisco, New York, Boston, London, Sydney, Tokyo: Academic Press, 2002: 715-724.

(9) Akki R, Desai P, Abhiraman AS. A framework for morphological evolution vis-à-vis phase transitions in polymer solutions. Journal of Applied Polymer Science 1999; 73(8):1343-1355.

(10) Nam YS, Park TG. Biodegradable polymeric microcellular foams by modified thermally induced phase separation method. Biomaterials 1999; 20(19):1783-1790.

(11) Nam YS, Park TG. Porous biodegradable polymeric scaffolds prepared by thermally induced phase separation. J Biomed Mater Res 1999; 47(1):8-17.

(12) Ho MH, Kuo PY, Hsieh HJ, Hsien TY, Hou LT, Lai JY, Wang DM. Preparation of porous scaffolds by using freeze-extraction and freeze-gelation methods. Biomaterials 2004; 25(1):129-138.

(13) Hu Y, Grainger DW, Winn SR, Hollinger JO. Fabrication of poly(alpha-hydroxy acid) foam scaffolds using multiple solvent systems. J Biomed Mater Res 2002; 59(3):563-572.

(14) Buschmann J, Muller E, Luger P. X-Ray Structure-Analysis of 1,4-Dioxane, Phase-I at 279-K and Phase-Ii at 153-K. Acta Crystallographica Section C-Crystal Structure Communications 1986; 42:873-876.

(15) Maquet V, Boccaccini AR, Pravata L, Notingher I, Jerome R. Preparation, characterization, and in vitro degradation of bioresorbable and bioactive composites based on Bioglass-filled polylactide foams. J Biomed Mater Res A 2003; 66(2):335-346.

(16) Blaker JJ, Gough JE, Maquet V, Notingher I, Boccaccini AR. In vitro evaluation of novel bioactive composites based on Bioglass-filled polylactide foams for bone tissue engineering scaffolds. J Biomed Mater Res A 2003; 67(4):1401-1411.

(17) Boccaccini AR, Notingher I, Maquet V, Jerome R. Bioresorbable and bioactive composite materials based on polylactide foams filled with and coated by Bioglass particles for tissue engineering application. Journal of Materials Science: Materials in Medicine 2003; 14:443-450.

(18) Tanaka H, Araki T. Phase inversion during viscoelastic phase separation: Roles of bulk and shear relaxation moduli. Physical Review Letters 1997; 78(26):4966-4969.

(19) Blasi P, D'Souza SS, Selmin F, DeLuca PP. Plasticizing effect of water on poly(lactide-co-glycolide). J Control Release 2005; 108(1):1-9.

(20) Maquet V, Boccaccini AR, Pravata L, Notingher I, Jerome R. Porous poly(alpha-hydroxyacid)/Bioglass composite scaffolds for bone tissue engineering. I: Preparation and in vitro characterisation. Biomaterials 2004; 25(18):4185-4194.

(21) Ma PX, Zhang R. Microtubular architecture of biodegradable polymer scaffolds. J Biomed Mater Res 2001; 56(4):469-477.

(22) Wang YW, Wu Q, Chen J, Chen GQ. Evaluation of three-dimensional scaffolds made of blends of hydroxyapatite and poly(3-hydroxybutyrate-co-3-hydroxyhexanoate) for bone reconstruction. Biomaterials 2005; 26(8):899-904.

(23) Ma PX, Choi J. Biodegradable Polymer Scaffolds with Well-Defined Interconnected Spherical Pore Network. Tissue Eng 2003; 7:23-33.

(24) Spaans CJ, Belgraver VW, Rienstra O, de Groot JH, Veth RPH, Pennings AJ. Solvent-free fabrication of micro-porous polyurethane amide and polyurethane-urea scaffolds for repair and replacement of the knee-joint meniscus. Biomaterials 2000; 21:2453-2460.

(25) Temenoff JS, Lu L, Mikos AG. Bone-Tissue Engineering Using Synthetic Biodegradable Polymer Scaffolds. In: Davies JE, editor. Bone Engineering. Hong Kong: Rainbow Graphic and Printing Ltd., 1999: 454-460.

(26) Schultz JM. Roles of solute and heat flow in the development of polymer microstructure. Polymer Reviews 1991; 32(18):3268-3283.

(27) Mandelkern L. Crystallization kinetics of homopolymers: overall crystallization: a review. Biophys Chem 2004; 112(2-3):109-116.

(28) Fischer EW, Sterzel HJ, Wegner G. Investigation of the structure of solution grown crystals of lactide copolymers by means of chemical reactions. Kolloid-Zeitschrift and Zeitschrift fur Polymere 1973; 251:978-990.